PHYSICAL REVIEW A VOLUME 39, NUMBER 1 JANUARY 1, 1989

Conical emission as a result of pulse breakup into solitary waves

M. E. Crenshaw and C. D. Cantrell
Center for Applied Optics, University of Texas at Dallas, Richardson, Texas 75083-0688

(Received 13 June 1988)

We report computational results that show that the conical emission observed when a nearly resonant laser pulse propagates through an atomic vapor is the result of the breakup of the pulse into solitary waves. For an incident pulse with a radial as well as a temporal profile, the crests and troughs of the two-dimensional solitary waves are curved in a time-radius plane. The temporal modulation associated with pulse breakup appears as Rabi sidebands in the spectrum, while the curvature of the solitary waves in the time-radius plane results in a transverse spatial modulation that leads to conical emission in the far field. These results were obtained by performing detailed numerical calculations of the time-dependent paraxial propagation of a cylindrically symmetric laser pulse through a vapor of two-level atoms under the rotating-wave and slowly-varying-envelope approximations in the limit of no collisional damping or Doppler broadening. Our results can be interpreted readily in terms of optical nutation on the Bloch sphere and in terms of noncollinear phase matching through the curvature of the solitary waves rather than through additional parametrically generated waves. We find that self-focusing is not required for the generation of conical emission, although it would be difficult to separate these effects experimentally.

I. INTRODUCTION

The interaction of intense, nearly resonant laser light with atomic or molecular systems has commanded the attention of researchers since the early 1960s because of the profound changes in the energy levels of the target systems and in their processes of emission and absorption induced by interaction with a strong field. The discovery and exploitation of effects such as the generation of new frequencies through interactions of nonresonant laser fields in matter ultimately led to methods for generating coherent light from the far infrared to the far ultraviolet, and played an important role in the development of laser spectroscopy. One of the signal successes of quantum optics in the 1970s was the quantitative and physical understanding of the interaction of an atom with a strong, nearly resonant laser field, in which the spontaneous fluorescence spectrum consists of two sidebands separated from a central peak by the Rabi frequency.[1] Stimulated processes such as gain and absorption are also modified as the result of interaction with a strong field. Gain has been observed by several workers at the Rabi sideband frequencies,[2,3] in agreement with theoretical predictions.[4,5] However, until fairly recently it has not been widely recognized that the generation of new frequencies by an atomic or molecular system interacting with a strong field is also interrelated with the propagation of this field in the medium. Observations of a frequency-shifted, coherent conical emission from systems pumped by an intense optical field that is nearly resonant with a one-photon transition[3,6–18] or a two-photon transition[19] have made it clear that propagation effects can play a major role in determining the spectrum as well as the spatial characteristics of the light transmitted by a medium subject to nearly resonant pumping. In this paper we provide answers to the following questions of primary interest: How are sidebands generated in conical emission, and how does the sideband frequency depend on experimentally adjustable parameters? What is the relationship between self-focusing and conical emission? How is phase matching accomplished in conical emission? The inadequacy of existing analytical methods in the face of the combined phenomena of coherent excitation, diffraction, and the initial spatial-temporal profile of the field has forced us to answer these questions by numerical calculation.

In the first observation of self-focusing due to the intensity-dependent dispersion of a resonance line, Grischkowsky[12] observed diffuse conical emission in potassium vapor. His analysis, which was based on the adiabatic approximation, was in agreement with the overall features of the observed self-focusing. Grischkowsky did not observe the spectrum of the conical emission, nor did he attempt an analysis of this phenomenon. Tam[3] observed sideband amplification and conical emission in a cw laser beam that was tuned to the blue side of the sodium D_2 line. Skinner and Kleiber[8] made a systematic study of the conical emission observed when barium vapor was irradiated with the beam of a nitrogen-laser-pumped dye laser tuned on the high-frequency side of a resonance line. The measured dependences of the cone angle on barium density and laser detuning were in semiquantitative agreement with a model in which the conical emission was the result of a surface-phase-matched four-wave-mixing process involving two other strong waves, the laser, and the cone light. However, the other two waves required for the model were not observed. Subsequently Harter *et al.*[7] and Kleiber, Burnett, and Cooper[20] observed sidebands that were symmetrically displaced with respect to the laser frequency, thus satisfying the condition for conversion of two pump photons into two sideband photons via a four-wave-mixing process. Harter and co-workers[6,7] described an optical-waveguide model showing how conical emission may originate in a four-wave-mixing process combined with refraction at the boundary of a self-trapped filament. A four-wave-mixing model, which relaxes the requirement for noncollinear phase matching in self-trapped filaments, has been discussed by Plekhanov *et al.*,[15] Shevy and Rosenbluh,[17] and Shevy, Hochman, and Rosenbluh.[18] Other models for the generation of conical emission which have been proposed include optical Čerenkov radiation,[8,14,16] spatial self-phase modulation,[21] self-defocusing of the lower sideband frequencies,[13] free-induction-decay emission following three-photon scattering,[17] a nonadiabatic generation process coupled with an optical-waveguide model,[11] and coupling between the field and the transient nonlinear response of the atomic system.[9,10,22] LeBerre-Rousseau, Ressayre, and Tallet[22] clearly recognized a possible link between conical emission and the proposal of Makarov, Cantrell, and Louisell[23] that sidebands would be coherently generated during propagation. However, the analytical methods of Ref. 22 were not sufficiently powerful to study the interplay between diffraction, the coherent response of the medium, and propagation effects. The observation by Chauchard and Meyer[13] that the symmetry rules that have been proposed with respect to the resonance and laser frequencies are valid only for a short detuning range and depend on scale parameters of the experiment supports the need for inclusion of all of the laser, material, and dimensional parameters into the theory.

Although a first-principles understanding of conical emission and sideband generation provides more than enough justification for a theoretical study, the possible importance of sideband generation as the result of propagation was first discussed in an applied context. A successful attack upon the problems of sideband generation and beam dispersal through self-focusing and conical emission may, in fact, be a prerequisite for major applications such as laser isotope separation[24] or plasma heating, in which a nearly resonant laser beam must traverse many optical depths of an atomic vapor. If a laser beam cannot propagate through long path lengths in the working medium without beam distortion, then an intended application that depends on uniform irradiation will not be feasible. The generation of unwanted new frequencies as the result of propagation might affect the isotopic or chemical selectivity of an industrial laser process, especially if the process relies upon excitation of sharp resonances. An early suggestion by Makarov, Cantrell, and Louisell[23] concerning the possible importance for multiphoton molecular excitation (and therefore molecular laser isotope separation) of the generation of sidebands in the course of propagation of a laser beam, rested on an analysis of the response of an individual two-level atom to an external field that was suddenly switched from zero to a finite value, E_0. Subsequent numerical work by Eberly, Konopnicki, and Shore[25] showed that the sidebands do not grow strongly in the course of propagation, and that the sideband amplitude depends sensitively on the initial rate of rise of the pulse. Numerical calculations by Cantrell, Rebentrost, and Louisell[26] showed that the sideband amplitude in the field radiated by the medium diminishes steadily in importance with respect to the amplitude at the frequency of the incident wave, as a function of propagation distance. In the sudden approximation employed by these two groups, the field E_0 at $t-n_0z/c=0$ is the initial condition for the solution of the differential equations describing the response of the atomic system to the field. Consequently, the field at the first retarded-time point can never be altered by the field emitted by the atoms over any distance of propagation, while the remainder of the pulse is substantially reshaped by propagation. Therefore the sudden approximation specifically forbids pulse delay, formation of solitary waves, and other self-induced transparency effects. For the examples of pulses with finite rise times studied by these authors, the distance of propagation considered was shorter than the reshaping distance. Finally, the restriction to a uniform plane wave excluded the development of phase-matched propagation at the sideband frequencies in other directions as required in several models of conical emission. In view of the expeirmental observations of sidebands and conical emission, the deficiencies of previous theoretical work[23,25,26] made it highly desirable to reevaluate the problem of sideband generation in the course of propagation.

In this article we report the results of a numerical study of the interrelated processes of coherent sideband generation and conical emission that occur as a pulse that is initially smooth and nearly adiabatic propagates through a vapor of statioary atoms with two effective energy levels. Our calculations show that a laser pulse the initial center frequency of which lies to the blue of the atomic resonance line undergoes radical changes in the course of propagation.[27,28] During the initial stage of propagation, the amplitude of the pulse envelope remains apparently little changed, while the initially plane phase front begins to carry a nonlinearly generated image of the intensity profile of the pulse as a result of the adiabatic response (self-phase modulation).[12,29,30] After an initial period of phase encoding, the radial variation in the field-induced refractive index becomes large enough for self-focusing[12,30] to become prominent. Self-steepening[29,31–33] of the pulse becomes evident on a length scale, independent of the self-focusing length, that is determined by the temporal variation of the field strength and phase. Eventually the pulse breaks up into a train of two-dimensional solitary waves, the leading edge of the pulse becoming steep and the pulse developing a strong temporal and transverse spatial modulation. A temporal-spatial spectrum shows the modulation associated with the train of two-dimensional solitary waves to be equivalent to Rabi sidebands and conical emission.

In our numerical model, the method for including transverse propagation effects such as diffraction and self-lensing as well as pulse reshaping in the time domain is to solve the paraxial wave equation for a unique helicity of the field with a driving term proportional to the polarization (exception value of the dipole moment per unit volume), the latter quantity being calculated directly by solving the appropriate dynamical equation. Atomic motion and collisions have been deliberately excluded in order to study, in as pure a form as possible, the phase-sensitive nonlinear processes arising from the interaction of two-level systems with a propagating laser field. One of the consequences of excluding collisions is that the time-dependent Schrödinger equation must be used to calculate the response of the atoms to the driving field, and its approximate solutions in the adiabatic and sudden regimes must be used to interpret the results. In the paraxial approximation, the wave equation is linear in the spatial and temporal derivatives of the optical field. When the laser frequency is nearly resonant with the transition frequency, the nonlinearity of the atomic polarization induced by the field couples the different frequencies present in the field, while new frequencies arise in the polarization because the coherent response of an atom to an external field depends on the atomic eigenfrequencies as well as on the frequency of the field. The approach of obtaining self-consistent solutions of the wave equation and the time-dependent Schrödinger equation (or the density-matrix equation of motion) was pioneered for plane waves and two-level systems by Hopf and Scully[34] and Icsevgi and Lamb[35] and extended to include transverse propagation effects by Newstein and coworkers.[36,37] Since this method does not make use of perturbative techniques such as the usual expansion of the dielectric susceptibility in powers of the optical field, it is valid under conditions of saturation and for resonant and nearly resonant excitation. The purpose of numerical calculation in this case is to reveal the essential physics, not to provide a simulation of experiment.

The generation of Rabi sidebands by an initially smooth pulse is a nonadiabatic, non-steady-state phenomenon. A laser pulse which evolves adiabatically, that is, sufficiently slowly that the atomic system remains in the dressed state correlated with the initial state, will not induce transitions to other dressed states. Then the dipole expectation value will contain no oscillations at the generalized Rabi frequency.[38] If the dipole expectation value induced by the propagating field contains no Rabi oscillations, then no Rabi sidebands will appear as the field propagates. In the steady-state approximation employed by Harter and Boyd[6] and LeBerre *et al.*[39] to calculate the atomic response to the field, the atom is assumed to be in dynamic equilibrium between collisions and coherent driving by the field. The index of refraction is intensity-dependent, but cannot generate Rabi oscillations since it follows the field envelope in time development. The presence of gain at the Rabi sideband frequencies permits the development of Rabi sidebands through the amplification of initial noise in cases where the steady-state approximation is valid, such as cw laser beams.[3]

At the entrance to the medium, the transient response of the two-level system is primarily adiabatic.[12,29,31] However, the atomic response also contains temporal oscillations, with an asymptotically small amplitude, at the instantaneous generalized Rabi frequency.[40] The retarded time of onset, the temporal frequency, and the number of temporal oscillations depend on the field strength, and therefore (for an incident beam of finite diameter) the radius, resulting in a curvature of the crests and troughs of the temporal oscillations in the time-radius plane. When the laser is detuned to the blue side of resonance, the frequency spectrum of the atomic response is asymmetric,[23,27,40–44] the lower sideband having a larger amplitude than the upper sideband. The degree of asymmetry increases with the radius. The temporal oscillations in the atomic response are impressed on the field during propagation because the source term in the paraxial wave equation is proportional to the atomic polarization. If changes in the field did not affect the atomic response (thin-sample approximation), then the effect of the atomic response on the propagating field would be cumulative with subsequent layers of the medium.[23] However, the amplitude of oscillations in the transient response increases during propagation because self-actions (including oscillations that have been encoded on the field over the distance through which it has already propagated) make the pulse less adiabatic. Therefore the process of encoding oscillations on the pulse is amplified as the pulse propagates. This process is a self-action of the electric field which we call "self-oscillation encoding".[27] Self-steepening and self-oscillation encoding eventually result in the breakup of the pulse into a train of solitary waves. With the inclusion of a radial dimension, the solitary waves become two-dimensional, with crests and troughs that are curved in the time-radius plane. The temporal oscillation associated with pulse breakup generates Rabi sidebands while the transverse dependence of pulse breakup results in a transverse spatial oscillation. We demonstrate that these interrelated oscillations are equivalent to Rabi sidebands and conical emission by calculating the temporal Fourier transform of the Hankel-transformed field. Since the Hankel field is the transverse spatial Fourier transform of the physical field, it is porportional to the physical field observed at a sufficiently large distance from the exit plane that the Fraunhofer approximation is valid.

After calculating the solution of the paraxial wave equation, we visualize the curvature of the solitary waves by arranging the uniform-plane-wave solutions for pulses with different initial field strengths along a radial coordinate in accordance with the initial field strength of an initially Gaussian transverse beam profile. The temporal-spatial spectrum demonstrates that Rabi sidebands and conical emission are generated, even though self-focusing and diffraction have been excluded in this approximation.

The remainder of this paper is divided as follows: In Sec. II we outline the derivation from first principles of the fundamental equations used in this work. The products of the significant effort expended to develop stable numerical methods that give reliable results for this problem are described in Sec. III. In Sec. IV we use the Bloch vector to give a physical interpretation of the dependence of the induced polarization on the laser-pulse profile and detuning. Section V summarizes and interprets in detail the results of a major numerical calculation of laser-pulse propagation. Our results are compared qualitatively with existing experimental results in Sec. VI.

II. EQUATIONS OF MOTION

We consider the propagation of a quasimonochromatic laser beam, initially in a TEM_{00} mode, through a medium with a background index of refraction n_0. Embedded in the medium are atoms or molecules with two energy levels connected by an electric dipole transition, the frequency ω_a of which is nearly equal to the laser frequency. To cast the problem in terms of propagating waves, one begins with Maxwell's equations; makes the paraxial approximation $\nabla(\nabla\cdot\mathbf{E})\approx 0$, which amounts to assuming that all wave vectors make no more than a small angle with the original axis of propagation; assumes a unique helicity (0 or ± 1) for the propgating field and the induced polarization; introduces slowly varying envelopes for the field and the polarization; and derives equations of motion for the envelope functions.[35,36] The resulting equation of motion for the field envelope E is, in Gaussian cgs units,

$$\left[\frac{\partial}{\partial z}-\frac{i}{2k_l}\nabla_T^2\right]E(\mathbf{r}_T,z,t')=\frac{2\pi k_l}{n_0^2}P(E(\mathbf{r}_T,z,t'))\ , \tag{2.1}$$

where the polarization envelope P is a functional of the electric field.[35,36] Propagation occurs in the $+z$ direction; $k_l=\omega_l n_0/c=2\pi n_0/\lambda$, where ω_l is the laser frequency and λ is the vacuum wavelength; $\mathbf{r}_T$ is the transverse coordinate; t' is the retarded time, $t'=t-n_0 z/c$; and ∇_T^2 is the transverse Laplacian. Assuming cylindrical symmetry, we define a dimensionless radius $\xi=r/r_c$, where r_c is an arbitrary characteristic radius. In terms of the dimensionless radial coordinate ξ, Eq. (2.1) becomes

$$\left[\frac{\partial}{\partial z}-\frac{i}{2k_l r_c^2}\nabla_{T,\xi}^2\right]E(\xi,z,t')=\frac{2\pi k_l}{n_0^2}P(E(\xi,z,t'))\ . \tag{2.2}$$

The Fresnel number is given by $F=\pi n_0 r_p^2/\lambda L$, where λ/n_0 is the wavelength in the medium, L is the propagation distance, $r_p=a_0(2\ln 2)^{1/2}$ is the radius half-maximum, and a_0 is the half-width $1/e$ point of the intensity. If the Fresnel number is much greater than one then the nonlinear interaction dominates the transverse effects.[4,37,45] In this case, the transverse Laplacian, which is responsible for diffraction and self-lensing, can be neglected and the equation of motion for the field envelope in cylindrical symmetry becomes

$$\frac{\partial}{\partial z}E(\xi,z,t')=\frac{2\pi k_l}{n_0^2}P(E(\xi,z,t'))\ . \tag{2.3}$$

This equation describes nonlinear propagation under the assumption that the propagation can be represented by a plane wave over small annular shells, where the initial field strength for each shell depends on the radius.[37,45]

If the interval δz is small enough that the polarization may be treated as constant, then the annular-plane-wave equation (2.3) can be linearized,

$$E(\xi,z+\delta z,t')\approx E(\xi,z,t')+\delta z\frac{2\pi k_l}{n_0^2}P(E(\xi,z,t'))\ . \tag{2.4}$$

Using this approximation, the field at $z+\delta z$ is obtained by multiplying the polarization by a small constant and adding it to the field at z.

In the rotating-wave approximation for a system with a ground state and one excited level interacting via an electric dipole transition with an external, classical, time-varying field

$$|E(\mathbf{r}_T,z,t')|\cos[-\omega_l t'+\phi(\mathbf{r}_T,z,t')]$$

(where the complex field envelope

$$E(\mathbf{r}_T,z,t')=|E(\mathbf{r}_T,z,t')|\exp[i\phi(\mathbf{r}_T,z,t')]$$

is supposed to vary slowly on the time scale of the period $2\pi/\omega_l$), the time-dependent Schrödinger equation takes the form[26,38,46]

$$\frac{\partial\tilde{c}_0}{\partial t'}=i\frac{\mu E^*(\mathbf{r}_T,z,t')}{2\hbar}\tilde{c}_1\ , \tag{2.5}$$

$$\frac{\partial\tilde{c}_1}{\partial t'}=i\frac{\mu E(\mathbf{r}_T,z,t')}{2\hbar}\tilde{c}_0+i\Delta\tilde{c}_1\ , \tag{2.6}$$

where Δ is the detuning of the laser frequency from resonance, $\Delta=\omega_l-\omega_a$; μ is the matrix element of the dipole operator; and $\tilde{c}_0$ and $\tilde{c}_1$ are the probability amplitudes of the ground state and excited state, respectively. The complex polarization is $P=2iN\mu\tilde{c}_0^*\tilde{c}_1$. Equations (2.5) and (2.6) are equivalent to the undamped optical Bloch equations. The complex polarization is related to the Bloch vector components u and v by the equation $P=iN\mu(u-iv)$.

III. NUMERICAL METHOD

A pseudospectral[47,48] method is used to propagate the field. In this method, a Hankel transformation of Eq. (2.2) converts the transverse Laplacian in cylindrical symmetry to an algebraic quantity, resulting in a first-order linear differential equation in z which is propagated using a midpoint-trapezoidal predictor-corrector. The source term is the Hankel transform of the polarization, which is most conveniently calculated by solving the time-dependent Schrödinger equation using the physical (not the transformed) field. A convolution of the source term is not practical in this case because the polarization is related to the solution of a set of coupled differential equations. Therefore, at each stage in the propagation, the propagated Hankel field is transformed into physical space, the polarization is calculated, and the resulting polarization is Hankel-transformed to act as the source term in the transformed propagation equation.

A Hankel-transform pair of order zero is defined as

$$\hat{f}(\lambda,z,t')=\int_0^\infty J_0(\lambda\xi)f(\xi,z,t')\xi\,d\xi\ , \tag{3.1}$$

$$f(\xi,z,t')=\int_0^\infty J_0(\lambda\xi)\hat{f}(\lambda,z,t')\lambda\,d\lambda\ , \tag{3.2}$$

where a circumflex has been used to denote the transformed function and the independent variables z and t' are shown explicitly. Applying the Hankel transformation to Eq. (2.2), one obtains

$$\left[\frac{\partial}{\partial z}+\frac{i\lambda^2}{2k_l r_c^2}\right]\hat{E}(\lambda,z,t')=\hat{R}(E(\xi,z,t')) , \tag{3.3}$$

where $R=2\pi k_l P/n_0^2$ is used to condense the notation. Making the transformation

$$\hat{E}(\lambda,z,t')=\hat{S}(\lambda,z,t')\exp(-i\lambda^2 z/2k_l r_c^2) \tag{3.4}$$

reduces Eq. (3.3) to

$$\frac{\partial}{\partial z}\hat{S}(\lambda,z,t')=\hat{R}(E(\xi,z,t))\exp(i\lambda^2 z/2k_l r_c^2) . \tag{3.5}$$

Denoting the z-step size of the finite-difference algorithm by h and defining $\Gamma=\exp(-i\lambda^2 h/2k_l r_c^2)$, we obtain the finite-difference equations for propagation by the midpoint-trapezoidal method,

$$\text{predictor:}\quad \bar{\hat{E}}_{n+1}=\hat{E}_{n-1}\Gamma^2+2h\hat{R}(E_n)\Gamma , \tag{3.6}$$

$$\text{corrector:}\quad \hat{E}_{n+1}=\hat{E}_n\Gamma+\frac{h}{2}[R(\bar{E}_{n+1})+\hat{R}(E_n)\Gamma] , \tag{3.7}$$

where a bar has been used to denote a predicted function. The Euler predictor and iterated trapezoidal corrector, respectively,

$$\hat{E}^{(0)}_{n=1}=\Gamma[\hat{E}_{n=0}+h\hat{R}(E_{n=0})] , \tag{3.8}$$

$$\hat{E}^{(k+1)}_{n=1}=\frac{h}{2}\hat{R}(E^{(k)}_{n=1})+\Gamma\left[\hat{E}_{n=0}+\frac{h}{2}\hat{R}(E_{n=0})\right] \tag{3.9}$$

are used to provide the starting values required for (3.6) and (3.7). The midpoint-trapezoidal method was chosen because it combines acceptable accuracy with currently attainable storage requirements.

The Hankel transformation is performed using a numerical formulation based on Gauss-Laguerre quadrature which was derived by Coffey, Lax, and Elliott.[47] The Bessel function in Eqs. (3.1) and (3.2) can be expanded in terms of the generating function[49]

$$J_0(\lambda\xi)\approx 2\exp[-(\xi^2+\lambda^2)/2]\sum_{m=0}^{M-1}(-1)^m L_m(\lambda^2)L_m(\xi^2) . \tag{3.10}$$

Equation (3.10) would be exact except that the infinite summation limit has been replaced by $M-1$ for numerical evaluation. The Guass-Laguerre quadrature formula is given by

$$\int_0^\infty f(x)e^{-x}dx\approx\sum_{j=1}^{M}f(x_j)w(x_j) , \tag{3.11}$$

where the $\{x_j\}$ are the abscissas of the Laguerre polynomial of order M and the $\{w(x_j)\}$ are the weights. This integration formula is exact for all polynomials of order $\leq 2M+1$. The substitutions $x=\xi^2$ and $y=\lambda^2$ convert the Hankel transformation given by Eq. (3.1) to

$$\hat{f}(\sqrt{y_i},z,t')\approx\sum_{j=1}^{M}f(\sqrt{x_j},z,t')\exp[-(y_i-x_j)/2] \times\sum_{m=0}^{M-1}(-1)^m L_m(y_i)L_m(x_j)w(x_j) , \tag{3.12}$$

which can be evaluated as the real-matrix–complex-vector product

$$\hat{f}(\sqrt{y_i},z,t')\approx\sum_{j=1}^{M}B_{ij}f(\sqrt{x_j},z,t') , \tag{3.13}$$

where f may represent either the field or polarization envelope. Because of the symmetry of Eqs. (3.1) and (3.2), Eq. (3.13) may be used for both the Hankel transformation and its inverse. The constant matrix B is calculated once accurately and stored for later use.[50]

This method of calculating the Hankel transform imposes a limit on the z-step size of $\delta z\lesssim 2k_l r_c^2/y_{\max}$ in order to minimize leakage into higher modes.[47] In practice, except for the most weakly nonlinear systems, the magnitude of the source term determines the z-step size by the requirement that the field not change appreciably in one z step. Although the magnitude of the source term is not expressible analytically and changes during propagation, the approximate magnitude can be obtained by evaluating the adiabatic approximation.[12,29,40,51] The standard technique of reducing step size until the results converge was used to verify consistency with this dynamic criterion for z-step size.

Performing a numerical spectral transformation introduces several types of errors, namely, roundoff, aliasing, and Gibbs's phenomenon. For any spectral method, an analytic transform of the field should be used to start the propagation.[52] This avoids introducing the aforementioned errors into the initial field, since they would otherwise propagate and be amplified. The initial field, Gaussian in time and radius, is

$$E(\sqrt{x_i},0,t')=E_0\exp\left[-\frac{x_i r_c^2}{2a_0^2}\right]\exp\left[-\frac{t'^2}{2\tau^2}\right] , \tag{3.14}$$

where we have assumed a focused beam which is purely real at the entrance to the media and where a_0 is the half-width $1/e$ point of the intensity. The analytic Hankel transform of Eq. (3.14) is

$$\hat{E}(\sqrt{y_i},0,t')=E_0\frac{a_0^2}{r_c^2}\exp\left[-\frac{y_i a_0^2}{2r_c^2}\right]\exp\left[-\frac{t'^2}{2\tau^2}\right] . \tag{3.15}$$

From Eqs. (3.14) and (3.15) it is apparent that the physical and Hankel fields are identical if $r_c=a_0$. Since the numerical grid is fixed by the square root of the abscissae of a Leguerre polynomial, the ratio r_c/a_0 determines the grid resolution of the field in transform space versus physical space. During nearly resonant propagation, the Hankel field spreads out while the physical field self-focuses (if $\Delta>0$) and develops radial oscillations. It is therefore appropriate to make r_c somewhat smaller than

a_0 in order to give adequate grid resolution in physical space.

During propagation, we are primarily concerned with roundoff error in the Hankel transformation because the Gaussian radial profile of both the field and the polarization makes aliasing and Gibbs's phenomenon negligible. Roundoff error is a problem for large values of the radial coordinate, where the field should fall off exponentially. At large radii, the unsmoothed physical field is composed entirely of roundoff error from the Hankel transformation. Since this error has random sign over the variable t', the error is amplified by the finite-difference solution for the polarization. Physically, over the range of parameters we use, the field should remain Gaussian in the transverse dimension at large radii. This condition is enforced by choosing a radial coordinate where the field still has appreciable magnitude and using the parameters of the original field along with the complex amplitude at the chosen coordinate to extrapolate the field:

$$E(\sqrt{x_i},z,t')=E(\sqrt{x_{i-1}},z,t')\exp\left[\frac{r_c^2}{2a_0^2}(x_{i-1}-x_i)\right] . \tag{3.16}$$

The transformation from the physical polarization to the Hankel polarization also suffers from roundoff error. In this case, the effect is not drastic since the polarization changes the propagating field only slightly in one z step. However, this error does accumulate after several propagation steps. To filter the error, we multiply the Hankel field every five z steps by a function that is approximately unity out to a chosen radial coordinate and then rapidly and smoothly decays to zero. Such a function is

$$\frac{1}{1+\exp[d(\sqrt{x_i}-\sqrt{x_0})]} ,$$

where d is the decay constant and $\sqrt{x_0}$ is the coordinate where the function has fallen to one-half.

In order to define the role of the transverse coupling which is responsible for diffraction and self-lensing, a second propagation program was written for the annular-plane-wave approximation, in which transverse coupling is excluded, Eq. (2.3). The field was propagated by the midpoint-trapezoidal predictor-corrector method in physical space rather than in transform space.

The numerical method used to calculate the polarization was presented in Ref. 40. This method is based on a multistep finite-difference method developed by Chu and Cantrell[53] for accurately solving differential equations with imaginary eigenvalues. Many well-known methods for solving systems of ordinary differential equations are actually unstable for equations with purely imaginary eigenvalues, such as the time-dependent Schrödinger equation, Eqs. (2.5) and (2.6).[53,54] Reference 40 also details techniques used to handle the improper initial conditions and the requirement of adiabaticity. A requirement for adiabaticity is $|\dot{E}/E| \ll |\Delta|$, which was met in Ref. 40 by adding a small constant field, called a pedestal, to the time-varying field. In this work we gave the pedestal a Gaussian transverse profile and increased the number of time points because the maximum generalized Rabi frequency increases during propagation as the result of self-focusing and self-steepening. To verify the accuracy of the solution, we checked the condition $0.9999 \le |\tilde{c}_0|^2+|\tilde{c}_1|^2 \le 1.0001$ at the end of each z step.

In as complex a calculation as this, questions inevitably arise about the correctness of a computer program that is intended to solve a given set of equations. We have checked the correctness of our program by comparing numerically computed free-space propagation with the analytical result; by comparing results obtained with our subroutine for the solution of the time-dependent Schrödinger equation with known analytical results; by hand calculation of selected points in the first step of propagation; and by a detailed examination of the computed field after propagation as described in Sec. V. The polarization subroutine used to obtain the results of this paper also produces the same results in time-dependent test cases in a completely independent propagation program[55] based on Drummond's algorithm.[56]

The computational effort required by our Hankel-transform propagation program depends on the parameters of the system under study. If M is the number of radial grid points and N is the number of time points, then M can range from 20 to 500 while N can range from ~ 100 (for free-space propagation) to several tens of thousands for a highly nonlinear system. Five $N \times M$ complex arrays are required to perform the Hankel transformation and to propagate the field. The number of floating-point operations required for a single Hankel transformation is proportional to M^2N. Finally, the number of z planes may range from ~ 10 to $\sim 10^3$. For a highly nonlinear system such as an atomic vapor driven near resonance, the number of floating-point operations required to model the propagation of a large-area pulse through a physically interesting propagation distance could exceed 10^{14}. It is clear that a vectorizing supercomputer is required for all but the most weakly nonlinear systems. The single calculation described in Sec. V required $\sim 6\times 10^{13}$ floating point operations taking approximately 140 CPU hours on a Cray X/MP-24.

IV. BLOCH-VECTOR BEHAVIOR

In the nearly adiabatic regime, the Bloch vector precesses in a narrow cone about the slowly evolving torque vector in Bloch space.[57] The half-opening angle α of the cone of precession is an asymptotically decreasing function of $|\Delta|\tau$, corresponding to an asymptotic approach[51,58] to the adiabatic limit in which the transition amplitude between the dressed states is zero and no new frequencies can be generated.[38] In the adiabatic limit,[12,29] the half-opening angle is zero; the adiabatic polarization is due solely to the time evolution of the torque vector. Finite orders of correction to the adiabatic approximation, which improve the accuracy of the approximation, can be derived.[29,31,40,51,59] A second-order approximation to the polarization is given by[40]

$$P_{(2)}=\frac{N\mu^2 w_{(2)}}{\hbar}\left[\frac{iE}{\Delta}+\frac{1}{\Omega'^2}\frac{dE}{dt'}+\frac{2i\beta E}{\Delta^2\Omega'^2}\right] , \tag{4.1}$$

where

$$w_{(2)}=\pm\left|\frac{\Delta}{\Omega'}\right|\left[1+\frac{\mu^2\Delta^2}{\hbar^2\Omega'^6}\frac{dE}{dt'}\frac{dE^*}{dt'}+\frac{4\beta}{\Delta\Omega'^2}+\left[\frac{8\Delta^2\hbar^2+4\mu^2|E|^2}{\hbar^2\Delta^2\Omega'^6}\right]\beta^2\right]^{-1/2} \tag{4.2}$$

is the second-order approximation to the inversion, $w=|\tilde{c}_1|^2-|\tilde{c}_0|^2$ (where the negative sign corresponds to an attenuator);

$$\Omega'(t')=[\Delta^2+\mu^2|E(t')|^2/\hbar^2]^{1/2} \tag{4.3}$$

is the instantaneous generalized Rabi frequency, which we take to be positive regardless of the sign of Δ; and

$$\beta(t')=\frac{i\mu^2}{4\hbar^2}\left[E\frac{dE^*}{dt'}-E^*\frac{dE}{dt'}\right] \tag{4.4}$$

is a purely real variable used to condense the notation. Unfortunately, the adiabatic approximation and its finite-order correction terms cannot adequately express the precession of the Bloch vector about the torque vector. The precession is significant because it induces oscillations in the polarization at the instantaneous generalized Rabi frequency.[40,57]

The trajectory of the Bloch vector is confined to the surface of the Bloch sphere.[57] When the torque vector changes direction very slowly compared with the rate of precession, the tip of the Bloch vector rotates in a plane defined by the intersection of the cone of precession with the surface of the Bloch sphere. Further, the plane of rotation must slowly change its orientation in order to follow the torque vector. The projections of the trajectory of the Bloch vector on the u and v axes give the in-phase and quadrature components of oscillation, respectively. For nonresonant pulses, the oscillations in the polarization must have both in-phase and quadrature components of amplitude because the plane of rotation is not parallel to the v-w plane in Bloch space.

The radius of the circle defined by the intersection of the cone of precession with the surface of the Bloch sphere is $\sin\alpha$. The projection of the circle onto the u-v plane results in an ellipse whose major semiaxis is $\sin\alpha$ and whose minor semiaxis is $(|\Delta|\sin\alpha)/\Omega'$.[41] The amplitudes of the in-phase and quadrature components of the real polarization are obtained by projecting the ellipse onto the u and v axes. When viewed from the origin, the Bloch vector rotates clockwise about the torque vector. Incorporating the rotation and the amplitudes, the oscillating portions of the Bloch vector components can be written as

$$u_{\rm osc}=-\sin\alpha\cos(\Omega't'+\zeta)\left[\frac{(\Delta/\Omega')^4+\tan^2\phi}{(\Delta/\Omega')^2+\tan^2\phi}\right]^{1/2} \tag{4.5}$$

and

$$v_{\rm osc}=\sin\alpha\sin(\Omega't'+\zeta)\left[\frac{(\Delta/\Omega')^4+\cot^2\phi}{(\Delta/\Omega')^2+\cot^2\phi}\right]^{1/2}, \tag{4.6}$$

where $\zeta(t')$ is a slowly varying phase. The complex polarization, $P=iN\mu(u-iv)$, becomes

$$P=P_0-\frac{iN\mu\sin\alpha}{2}\left\{\left[\left[\frac{(\Delta/\Omega')^4+\cot^2\phi}{(\Delta/\Omega')^2+\cot^2\phi}\right]^{1/2}+\left[\frac{(\Delta/\Omega')^4+\tan^2\phi}{(\Delta/\Omega')^2+\tan^2\phi}\right]^{1/2}\right]e^{i(\Omega't'+\zeta)}-\left[\left[\frac{(\Delta/\Omega')^4+\cot^2\phi}{(\Delta/\Omega')^2+\cot^2\phi}\right]^{1/2}-\left[\frac{(\Delta/\Omega')^4+\tan^2\phi}{(\Delta/\Omega')^2+\tan^2\phi}\right]^{1/2}\right]e^{-i(\Omega't'+\zeta)}\right\}, \tag{4.7}$$

where P_0 is the contribution of the nonoscillating components arising from the evolution of the torque vector. For a purely real field, Eq. (4.7) reduces to

$$P=P_0-\frac{iN\mu\sin\alpha}{2}\left[\left[1+\frac{\Delta}{\Omega'}\right]e^{i(\Omega't'+\zeta)}-\left[1-\frac{\Delta}{\Omega'}\right]e^{-i(\Omega't'+\zeta)}\right]. \tag{4.8}$$

As a function of the retarded time, the half-opening angle for a nearly adiabatic pulse with sufficiently large pulse area has three distinct regimes of behavior, but is relatively constant within each regime.[40] Note that the oscillating components have constant amplitude only when the field strength and phase are constant, as in the center portion of an adiabatic square pulse.

While derived in the context of near adiabaticity, Eqs. (4.5) through (4.8) apply to any system governed by Eqs. (2.5) and (2.6) over any portion of the time axis for which the torque vector changes direction slowly on the time scale of the generalized Rabi period. For example, in the sudden approximation $P_0=-\Delta\mu E_0/\hbar\Omega'^2$, $\zeta=\pi$, $\sin\alpha=\mu E_0/\hbar\Omega'$, and $\phi=0$ given the initial conditions $w_0=-1$ and $u_0=v_0=0$ for an unchirped pulse.

Since the emitted field is proportional to the complex polarization, the power spectrum of the emitted field in the thin-sample approximation as a function of the detuning $\Delta\omega$ from the laser frequency can be approximated by

$$I(\Delta\omega)\approx\frac{4\pi^2k_l^2(\delta z)^2}{n_0^4}\left|\int_{-\infty}^{\infty}P(t')e^{i\Delta\omega t'}dt'\right|^2, \tag{4.9}$$

which yields spectral sidebands corresponding to the exponentials $e^{\pm i\Omega't'}$ in Eqs. (4.7) and (4.8). From the coefficients multiplying the exponentials, it is apparent that the sideband on the resonance side of the center frequency is larger than the opposite sideband. Courtens and Szöke rigorously derived the asymmetric spectrum of the emitted field using a similar model in the adiabatic-square-pulse approximation.[41] However, it should be emphasized that the sideband asymmetry in the transient spectrum is a result of the nonzero value of Δ/Ω' and is not a result of adiabaticity. Sideband asymmetry has been predicted in the sudden approximation[23,42,43] as well as in the nearly adiabatic regime.[41,44] Limiting cases of Eqs. (4.7) and (4.8) include the high-Rabi-frequency–small-detuning limit, where the sidebands are totally symmetric, and the low-Rabi-frequency–large-detuning limit, where a single resonant sideband appears.[40–44] Equations (4.7) and (4.8) apply only to transient excitation; however, sideband asymmetry has been predicted in the steady-state spectrum for partially coherent excitation where transiency is continually reinitiated by phase fluctuations.[60,61] The sidebands generated by precession of the Bloch vector correspond to temporal oscillations and should not be confused with sidebands caused by simple reshaping of the pulse.

A system starting in the ground state in the infinite past and returning to the ground state in the infinite future defines an eigenvalue problem for the pulse area governed by the time-dependent Schrödinger equation (or the undamped optical Bloch equations).[40] For a nonresonant Gaussian pulse, the pulse-area eigenvalues of the time-dependent Schrödinger equation depend on $|\Delta|\tau$, but are less than the $2n\pi$ bound-state eigenvalues[62,63] of the cubic or nonlinear Schrödinger equation. The preeminent position of the hyperbolic-secant pulse shape in laser pulse propagation theory is partially due to the fact that the pulse-area eigenvalues are equal to $2n\pi$ for all values of detuning and time constant.

A typical trajectory of the Bloch vector for a temporally Gaussian pulse was calculated using the numerical method presented in Ref. 40. The parameters for this calculation were: detuning from resonance $\Delta\nu = 15$ GHz; time full width at half maximum (FWHM), 0.125 ns ($\tau = 0.0531$ ns); peak field strength $E_0 = 47.1$ statvolts/cm; pedestal, 9.42×10^{-3} statvolts/cm; dipole transition moment $\mu = 8.49\times10^{-18}$ statcoulomb cm; and total pulse area $\Theta = 50.4$ $(8.02\times2\pi)$ rad. The detuning was made small enough that the nonadiabatic effects would be visible in graphs. A perpendicular polar projection of the numerical calculation of the trajectory is shown as a solid line in Fig. 1. The dashed line is the projection of the trajectory of the second-order approximation to the polarization (4.1) divided by $N\mu$ so that it also is confined to the surface of the Bloch sphere. At $t' = -\infty$, the Bloch vector is antiparallel to the polar (w) axis. As the field strength increases, the trajectory of the Bloch vector nearly coincides with the second-order approximation. Significant departure from the latter approximation occurs as the instantaneous pulse area,

$$\theta(t') = \int_{s=-\infty}^{s=t'} \frac{\mu E(s)}{\hbar} ds , \tag{4.10}$$

increases to the point where it is a significant fraction of the first pulse-area eigenvalue[40] of the time-dependent Schrödinger equation (undamped optical Bloch equations). As the field strength continues to increase, the pulse area increases at a faster rate and the Bloch vector begins to precess rapidly about the torque vector. The precession induces oscillations in the polarization, which we call "central oscillations,"[40] as shown at the bottom of Fig. 1. The number of central oscillations is one less than the number of pulse-area eigenvalues that are less than the total pulse area. Since the central oscillations have components of amplitude along both the u and v axes, the sidebands resulting from these oscillations are asymmetric. The oscillations that occur in the tail of the pulse,[40] which are also due to precession of the Bloch vector, behave very differently than the central oscillations. The amplitude of the tail oscillations exhibits zeros when the total pulse area Θ is a pulse-area eigenvalue.[40] If the total pulse area is not a pulse-area eigenvalue, then the tail oscillations are responsible for an irreversible transfer of energy to the medium as "radiation."[62,63] After the pulse has passed, the Bloch vector precesses indefinitely about the inversion axis so that the tail oscillations continue indefinitely as a constant-amplitude rotation about the pole, yielding a single resonant sideband since the in-phase and quadrature components of the oscillation have equal amplitudes. Exact solutions have

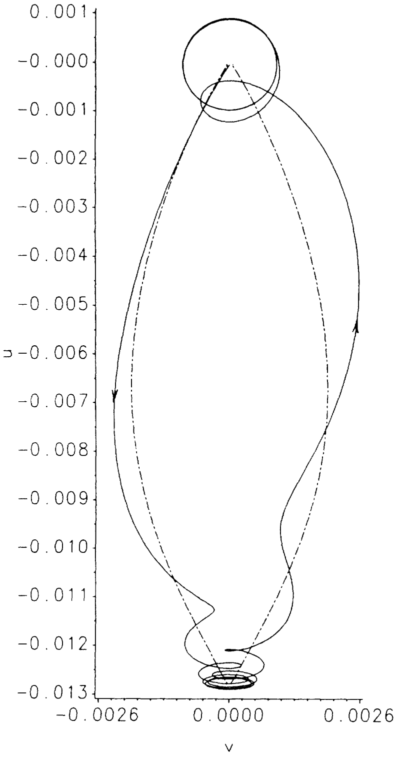

FIG. 1. Perpendicular polar projection of the trajectory of the Bloch vector. The solid line corresponds to the numerical solution of the time-dependent Schrödinger equation. The dashed line is the second-order approximation. The starting point for the trajectory is the polar (w) axis located at (0,0) in the figure. The arrowheads define the direction of the trajectory.

been derived for the behavior of the tail oscillations in the low-Rabi-frequency limit $[w(t')=-1]$.[40] In this limit, the imaginary part of the polarization is equivalent to the response of a simple harmonic oscillator to a Gaussian forcing function. In fact, any single-peaked time-dependent forcing function that begins at $t'=-\infty$ should cause a simple harmonic oscillator to begin oscillating at the temporal peak of the forcing function.

An additional type of oscillatory behavior occurs when a pulse is started at a finite time. Crisp[51] has derived an exact solution in the low-Rabi-frequency (simple harmonic oscillator) limit for the γ-distribution pulse $E(t')=E_0 t'^2\exp(-t'/\tau)/\tau^2$ with $t'\geq 0$. These "initialization oscillations" have been deliberately excluded from our calculations by using the adiabatic approximation as the initial condition.

It is worthwhile to consider the results of this section in the context of the ubiquitous sudden approximation. We assume $\phi(t')=0$ and the initial conditions $w_0=-1$ and $u_0=v_0=0$. In the low-Rabi-frequency limit, initialization oscillations begin at $t'=0$ and continue indefinitely at the detuning frequency with constant amplitude. For nonzero Rabi frequencies, there are no initialization oscillations; central oscillations at the generalized Rabi frequency begin at $t'=0$ and continue until the pulse is switched off. For the square pulse, the central oscillations are known as Rabi oscillations, resonance fluorescence, or optical nutation,[64] depending on the context. If any population remains in the excited state when the pulse is switched off, then tail oscillations at the detuning frequency continue indefinitely. If there is no population in the excited state, then the amplitude of the tail oscillations is zero and the total pulse area is a pulse-area eigenvalue. Pulse-area eigenvalues for the sudden approximation are $2n\pi\mu E_0/\hbar\Omega'$ since the system is returned to the ground state at $\Omega' t'=2n\pi$. For square-pulse excitation, the tail oscillations correspond to the free-induction signal. This is not true for a general pulse shape, because the tail oscillations can begin at any local maxima of the field strength and are associated with the inertia of the system (to this point, we have considered only single-peaked functions for the field strength). The field strength can have significant magnitude, and therefore the oscillations cannot be considered to be "free." Square-pulse excitation is not considered further because, as argued in the introduction, it is not physical for the propagation of a laser pulse.

The diverse types of Bloch vector behavior are significant generalizations of Rabi oscillations and optical nutation. All of the oscillatory types of behavior are capable of causing population pulsations,[65] the amplitude of which depends on the cone opening angle and the angle between the torque vector and the inversion axis. Population pulsations are most significant where the field strength is largest and therefore will be dominated by the central oscillations when the pulse area is large enough for this type of behavior to occur.

It should be noted that only the temporal behavior of the Bloch vector has been considered in this section. Physically important phenomena also depend on the transverse and longitudinal position in the medium.

V. LASER-PULSE PROPAGATION

In this section we present the results of numerical propagation of a laser pulse that is initially Gaussian in time and radius. We used the following parameters: resonance frequency $\nu=509$ THz (wavelength $\lambda=589$ nm); detuning from resonance $\Delta\nu=60$ GHz ($\Delta\lambda=0.0694$ nm); spot size $a_0=0.0186$ cm; radial scaling constant $r_c=a_0/5$; time FWHM, 0.125 ns ($\tau=0.0531$ ns); peak field strength $E_0=47.1$ statvolts/cm (intensity $=265$ kW/cm^2); on-axis pedestal, 9.42×10^{-3} statvolts/cm; dipole transition moment $\mu=8.49\times 10^{-18}$ statcoulomb cm; on-axis total pulse area $\Theta=50.4$ ($8.02\times 2\pi$) rad; number density $N=4\times 10^{14}$ cm^{-3}; background index of refraction $n_0=1$; longitudinal step size, 9.375×10^{-4} cm; time-step size, 25.4 fs; number of Gauss-Laguerre basis functions, 375. The resonance frequency and dipole moment are approximately those for the $(3\,^2S_{1/2}-3\,^2P_{3/2})$ D_2 transition of Na. The focused Gaussian field incident on the attenuating medium is shown in Fig. 2.

The Fresnel number is large for appropriately small propagation distances, regardless of the magnitude of any other parameters. Therefore, in the initial stage of propagation, each annulus evolves in accordance with the uniform-plane-wave approximation.[4,37,45] In order to understand the basic phenomena occurring during propagation, it is useful to consider the linearized annular-plane-wave equation (2.4), which is equivalent to solving the annular-plane-wave equation (2.3) with an Euler-predictor numerical method. In this method, the complex polarization is calculated from the known field at the current layer of the medium, multiplied by a small constant proportional to the longitudinal step size, and added to the known field to obtain the field at the succeeding layer of the medium. Considered as a numerical method, the Euler predictor is weakly unstable and is not particularly accurate. However, it is useful for a qualitative understanding of the mechanisms by which many nonlinear processes modify the propagating field.

At the entrance to the medium, the field is purely real. The second-order approximation to the polarization given by Eq. (4.1) reduces to a symmetric, purely imaginary portion and a smaller, antisymmetric, purely real portion for the Gaussian temporal profile. Applying the Euler predictor by adding the symmetric, purely imaginary portion of the polarization, multiplied by a small constant, to the field induces a temporally and radially dependent phase that is approximately a scaled image of the intensity of the field. The scaled image is concave downward for positive detuning but would be concave upward if the detuning were negative. The real part of the polarization is proportional to the derivative of the field and is positive before the peak and negative after the peak. The Euler predictor also permits us to see that self-steepening[29,31,32] occurs because the field strength is increased before the peak and decreased after the peak.

As self-phase modulation[30] causes the field to become complex, the polarization acquires additional phase-modulation and reshaping terms that are treated in more detail in Appendix A, where we use the second-order ap-

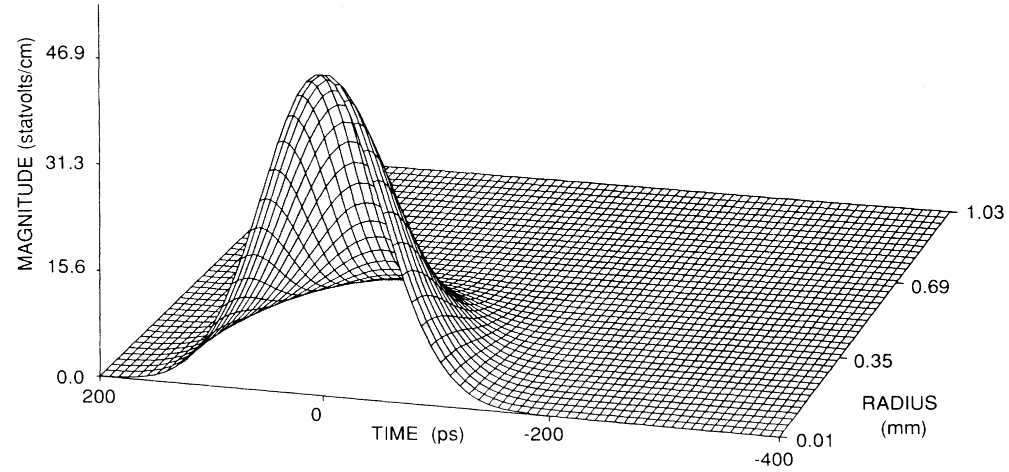

FIG. 2. Incident Gaussian field.

proximation to the polarization (4.1) to gain physical insight into the initial stages of pulse distortion.

Next we consider the effects of higher-order terms in the polarization.[40] For nearly adiabatic pulses, the oscillations that were discussed in Sec. IV are generally too small in relation to the total polarization to be visible in graphs. However, the small-scale structure in the polarization can be obtained by subtracting a known approximate polarization from the total polarization, which must be calculated numerically. For the parameters used in this problem, subtracting a fourteenth-order approximation from the total polarization does not reveal sufficient detail for this discussion. Therefore, for illustrative purposes, we present Fig. 3 which is typical of the real part of the higher-than-fourteenth-order polarization at the entrance to the medium, but with the detuning reduced to 41 GHz. This figure demonstrates the radial dependence of the Rabi oscillations as a result of the transverse variation in field strength. In Fig. 3, the retarded time of onset of the temporal oscillations increases in the radial dimension because it takes more retarded time for the pulse area to integrate to the first pulse-area eigenvalue as the peak field strength decreases. The spacing between temporal crests and troughs increases with radius because of a decrease in the temporal frequency $\Omega'(\xi,z=0,t')$. The number of central oscillations is also a decreasing function of radius because of the decreasing pulse area. Thus, the retarded time of onset, the temporal frequency, and the number of the temporal oscillations depend on the field strength, and therefore the radius, resulting in the curvature of the crests and troughs of the central oscillations in the time-radius plane as shown in Fig. 3. The radial dependence of the temporal oscillations is equivalent to a transverse spatial oscillation as can be observed in Fig. 3 by following an isochronic line in the radial direction. The zeros of the tail oscillations at the pulse-area eigenvalues are clearly visible as the pulse area decreases in the radial dimension. The imaginary part of

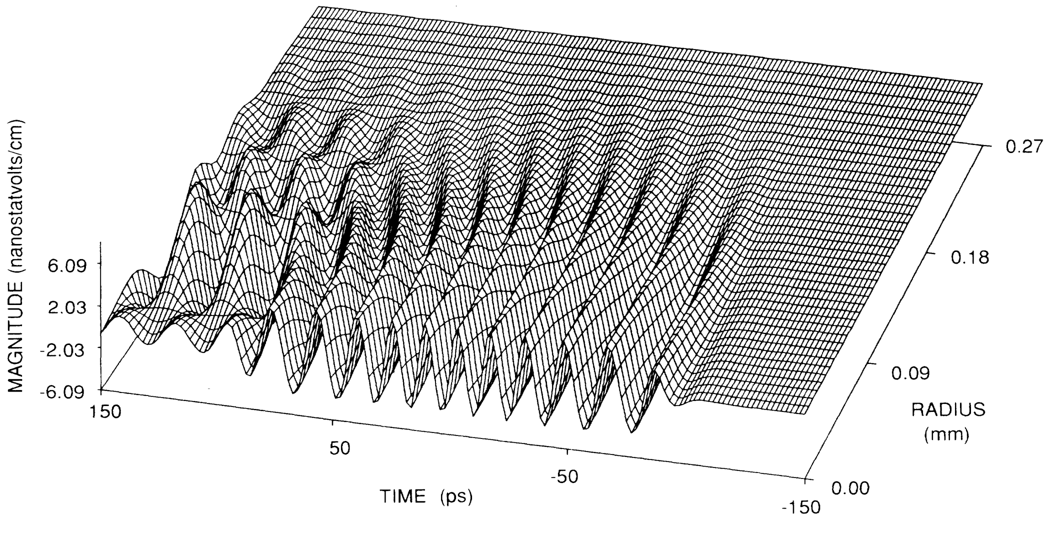

FIG. 3. Real part of the higher-than-fourteenth-order polarization at the entrance to the medium.

the polarization has corresponding oscillations as described in Sec. IV. When the radial dependence is included in the ratio of the amplitudes of the two quadratures, Eq. (4.8) shows that sideband asymmetry increases in the radial dimension as the ratio $|\Delta|/\Omega'$ approaches unity.[41-44]

Again applying the Euler predictor, we multiply the temporally and spatially oscillating polarization by a small constant and add it to the field. Therefore, even at the first longitudinal step into the medium, the field has a small component of conical emission due to the temporal-spatial oscillations that are present in the polarization at the entrance to the medium. This is the first step in the process we call "self-oscillation encoding" by which temporal-spatial oscillations appear in the field.[27]

If the oscillations in the polarization were to remain unchanged during propagation (as is assumed to be true under the thin-sample approximation), then the effect of self-oscillation encoding on the field would be cumulative with subsequent layers of the medium.[23] However, the amplitude of the oscillations in the polarization increases as the pulse propagates because self-phase modulation, self-steepening, and self-oscillation encoding cause the pulse to become less adiabatic. Therefore self-oscillation encoding is amplified during propagation. After a sufficiently long distance of propagation, self-oscillation encoding and self-steepening result in pulse breakup into macroscopic solitary waves.[27,40,66] The central oscillations in the polarization can be characterized as solitary-wave precursors (precursors of pulse breakup into solitary waves) because of their relationship to the pulse-area eigenvalues of the time-dependent Schrödinger equation, to the bound-state eigenvalues of the nonlinear Schrödinger equation, and to pulse breakup into solitary waves. Since the pulse is of finite extent in both radius and time, a train of two-dimensional solitary waves which includes a transverse spatial frequency as well as a temporal frequency is generated.

Self-oscillation encoding also applies to uniform plane waves. In the case of a resonant uniform plane wave, self-oscillation encoding results in the breakup of the pulse into the well-known one-dimensional solitons of self-induced transparency.[62,63,67-69]

We next consider numerical propagation of the pulse using the accurate pseudospectral method described in Sec. III. Figure 4 shows the phase of the complex field at the first z step ($z=9.4\times10^{-4}$ cm). We have already discussed the effects of the second-order approximation to the polarization. The portion of the phase that is concave upward in time is a result of higher-than-first-order terms in the polarization and the step on the right-hand side of Fig. 4 results from the small pedestal that is added to the field to ensure that the numerical method starts adiabatically.[40,41] Diffraction results in a parabolic curvature of the phase in the radial direction. This curvature is present in Fig. 4 but is so small that it cannot readily be discerned without truncating the intensity-dependent portion of the phase and rescaling. A transverse energy flow

$$J_T=\frac{1}{k_l}|E|^2\frac{\partial\phi}{\partial r}\ , \tag{5.1}$$

where $E=|E|e^{i\phi}$, is associated with the radial variation of the phase of the complex field envelope.[36,37,45] Diffraction (which gives a positive transverse gradient) is clearly dominated by the nonlinear interaction (which in this case gives a negative transverse gradient) as is the case for all experimental observations of conical emission of which we are currently aware.

Although all nonlinear effects are active from the entrance to the medium, the amplitude of the pulse envelope appears little changed throughout the initial stage of propagation. During this period, the most important nonlinear process is self-phase modulation, in which the nonlinearly generated approximate image of the intensity profile of the pulse in the phase front grows as a result of the adiabatic response. As a result of this initial period of phase encoding, the transverse gradient of the phase becomes large enough for self-focusing[12,30,70] to become evident.[36,37,45] Similarly, the dependence of the phase on time changes the instantaneous frequency at different re-

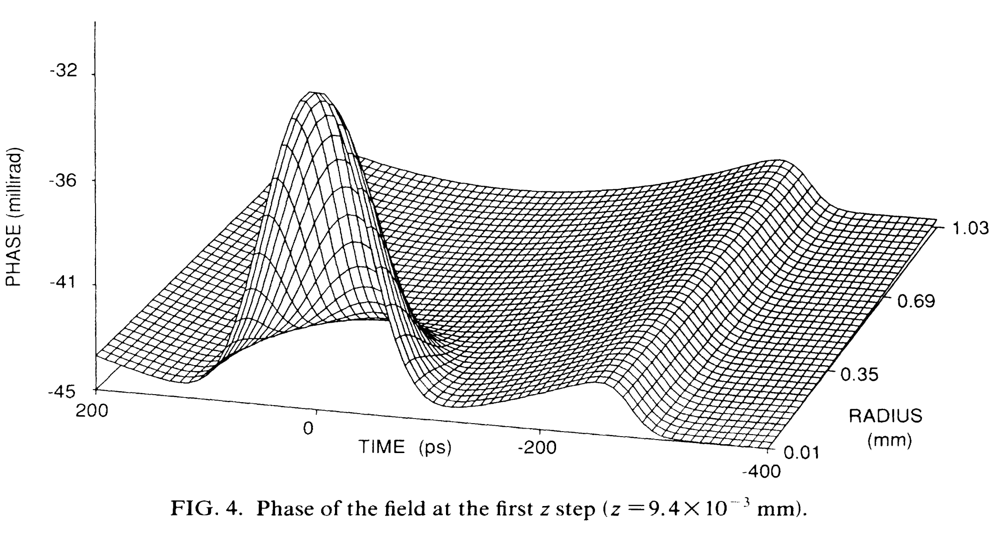

FIG. 4. Phase of the field at the first z step ($z=9.4\times10^{-3}$ mm).

tarded times, leading to group-velocity dispersion and thereby enhancing the self-steepening process that began at the entrance to the medium.[29,31,33] Self-steepening is further amplified by the change in the temporal variation of the field strength as the pulse propagates. Self-steepening shifts the temporal peak forward of the centroid of the pulse area, the shift being less pronounced as the radius increases because the nonlinear response diminishes as the field strength decreases.

Initially the amplitude of the oscillations in the polarization is an asymptotically small function of $|\Delta|\tau$. Therefore self-oscillation encoding begins slowly, even more slowly than self-steepening and self-focusing, apparently having little effect on the shape of the pulse. However, like the processes that amplify self-steepening and self-focusing, the processes that amplify self-oscillation encoding become more important throughout the initial stages of propagation. Eventually the combination of self-steepening, self-oscillation encoding, and self-phase modulation make the pulse sufficiently nonadiabatic for self-oscillation encoding to begin to play a significant role in pulse reshaping. At the leading edge of the pulse, the solitary-wave precursors add coherently in z. Because pulse reshaping and self-focusing alter the instantaneous generalized Rabi frequency along the pulse, the degree of coherence decreases along the temporal length of the pulse. As a result, pulse breakup begins as a small ripple in the magnitude at the leading edge of the field and in the near-axis region where the field strength is largest. The magnitude of the field at $z = 2.81$ mm (300 z steps) is shown in Fig. 5.

As pulse breakup continues, the region in which the ripple in the magnitude of the field is perceptible spreads to larger radii and later retarded times while the depth of modulation increases in the forward, nearly axial region where pulse breakup began. The magnitude of the field at $z = 3.75$ mm (400 z steps) is shown in Fig. 6 while Fig. 7 shows the truncated temporal-spatial spectrum (time-Fourier transform of the Hankel field) at the same propagation distance. Note that the lower sideband frequencies are shown on the right side of the temporal-spatial spectrum to expose detail. Pulse breakup is a temporal oscillation which appears as Rabi sidebands in the temporal spectrum. There are no appreciable radial oscillations in Fig. 6 so that the spatial spectrum is concentrated at small transverse wavenumbers.

Because the field strength decreases in the radial dimension, as the radius increases it takes more retarded time for the integrated pulse area to reach that needed to form a solitary wave. Therefore temporal retardation of the leading edge of the pulse increases with radius, resulting in a curved pulse front in the time-radius plane. Similarly, the spacing between solitary waves increases with radius. This is the analog of Fig. 3 for the propagation problem. The curvature is further enhanced during propagation because the field is more intense near the axis and therefore propagates faster and because more self-steepening occurs near the axis. Since pulse breakup has extended to large radii, at which the sidebands are quite asymmetric, the lower sideband grows more than the upper sideband and at significantly large transverse spatial wavenumbers because of the curvature of the solitary waves in the time-radius plane. The magnitudes of the field and the temporal-spatial spectrum at this stage of propagation, $z = 5.16$ mm (550 z steps), are shown in Figs. 8 and 9, respectively. The temporal-spatial oscillations in the complex field result in a frequency-shifted, angularly displaced peak in the temporal-spatial spec-

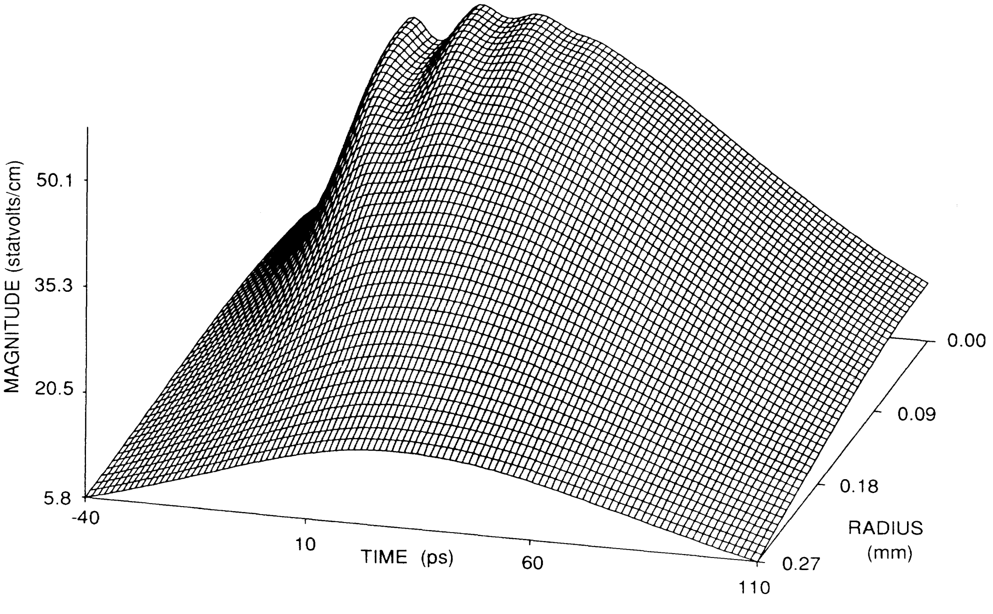

FIG. 5. Magnitude of the transmitted pulse at $z = 2.81$ mm (300 z steps). The origin in time is referenced to the center of the pulse at $z = 0$.

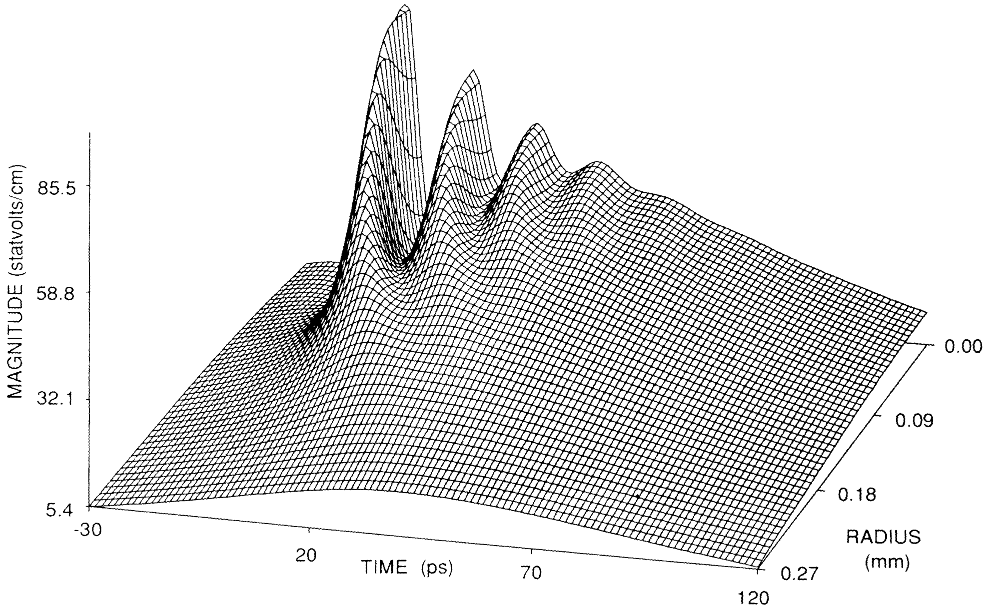

FIG. 6. Magnitude of the transmitted pulse at $z = 3.75$ mm (400 z steps).

trum at -44.62 GHz and 889 cm^{-1} which we identify as conical emission. The half-opening angle of the conical emission is given by

$$\theta_c = \tan^{-1}\left[\frac{k_\perp}{k_\parallel}\right] = 0.477^\circ . \tag{5.2}$$

As pulse breakup becomes fully developed in the near-axis region at the front part of the pulse, the fully developed solitary waves begin to behave as temporally independent pulses. Self-oscillation encoding has little effect on the leading, independent solitary waves because this process requires a larger pulse area. However, it begins to act more effectively on the latter portion of the pulse since, in effect, there is a new leading edge. Each fully developed solitary wave now propagates independently. The most intense solitary waves at the beginning of the pulse propagate fastest, spreading out the temporal oscillations and causing the sidebands to move toward the center frequency. The portion of the solitary waves

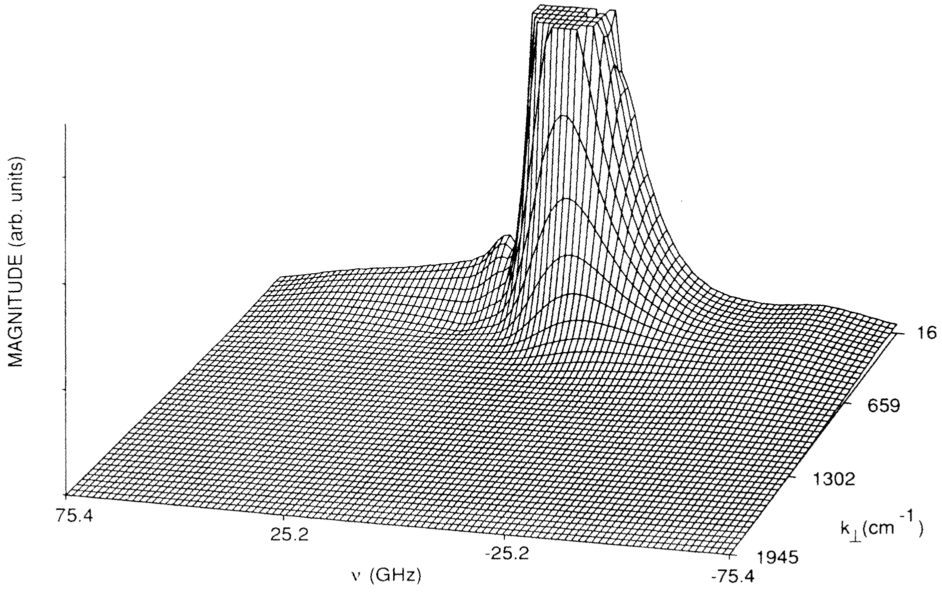

FIG. 7. Truncated temporal-spatial spectrum of the transmitted pulse at $z = 3.75$ mm (400 z steps). The incident laser frequency is at zero.

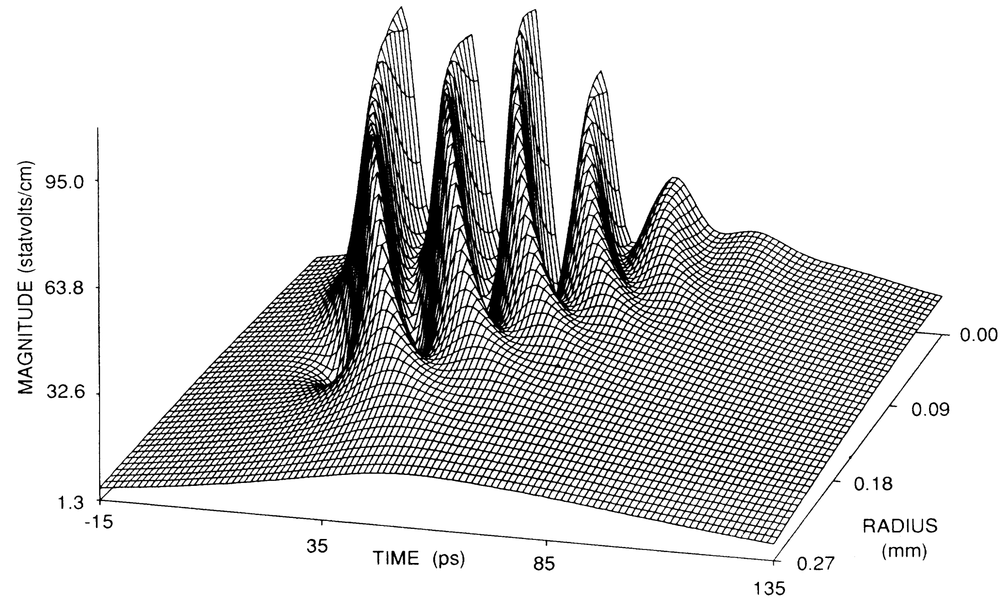

FIG. 8. Magnitude of the transmitted pulse at $z = 5.16$ mm (550 z steps).

near the axis propagates faster than the less intense portion far away from the axis, thereby causing the conical-emission peak to move outward to higher wavenumbers. This increase in transverse spatial wavenumber is accentuated by whole-beam self-focusing, which increases the rate at which the pulse area changes in the radial direction and, in addition, makes the near-axis solitary waves even more intense, thereby amplifying the difference in propagation speed with respect to the radial dimension. The magnitude of the field and the temporal-spatial spectrum at this stage of propagation, $z = 6.56$ mm (700 z steps), are shown in Figs. 10 and 11. The transverse spatial wavenumber of the conical emission has increased to 1195 cm^{-1} and the magnitude of the temporal frequency of conical emission has decreased with the peak now appearing at -32.2 GHz. The half-opening angle of the conical emission is now 0.642°. Since the pulse has become fully modulated, the amplitude of the spectral component of conical emission has become saturated and cannot grow significantly with further propagation.

The time development of the magnitude of the Hankel field at $z = 6.56$ mm (700 z steps) is shown in Fig. 12.

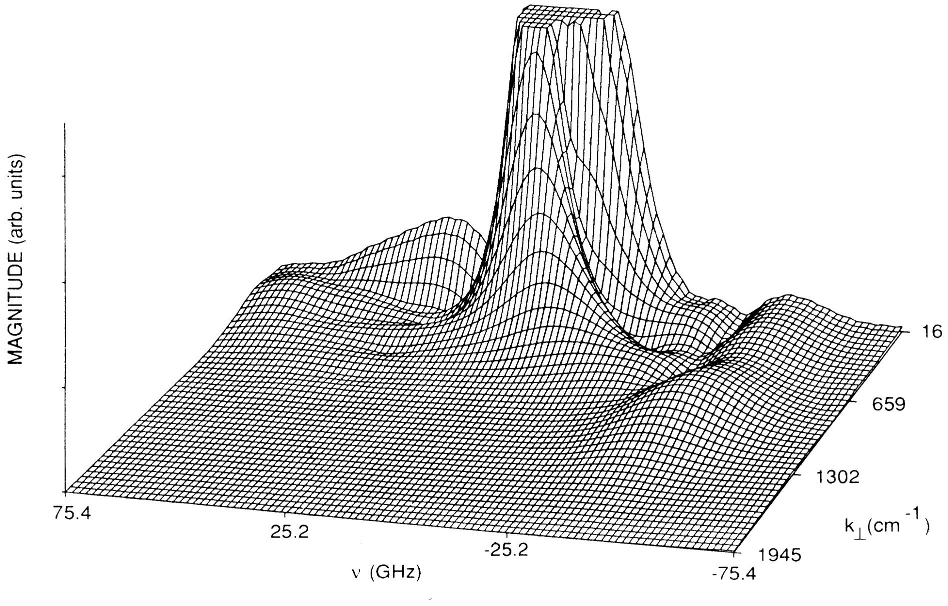

FIG. 9. Truncated temporal-spatial spectrum of the transmitted pulse at $z = 5.16$ mm (550 z steps).

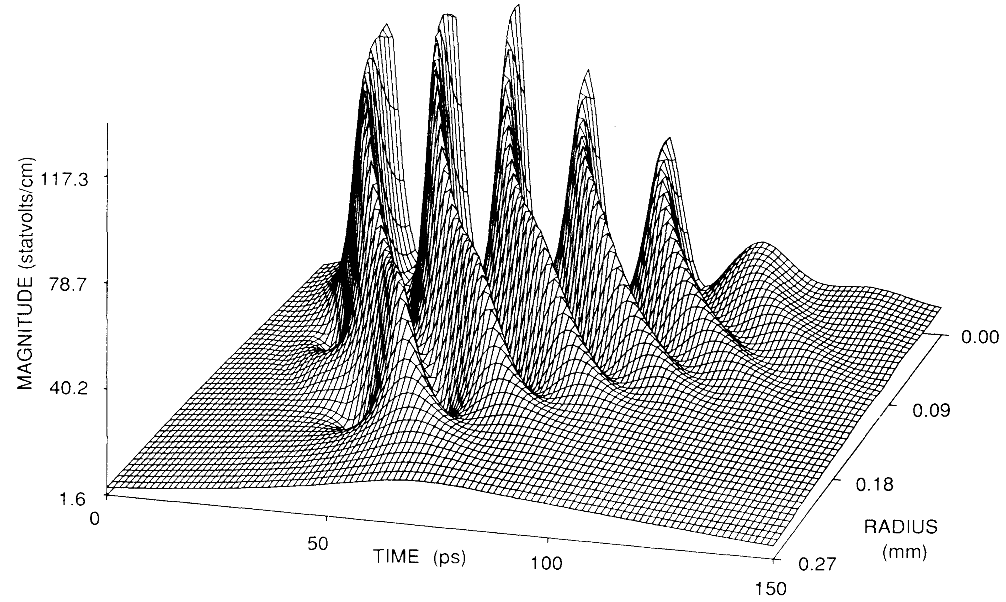

FIG. 10. Magnitude of the transmitted pulse at $z = 6.56$ mm (700 z steps).

The peak is concentrated at small spatial wavenumbers. At the leading edge of the physical field, there is a wide distribution of spatial wavenumbers. Subsequently, the Hankel field develops a well-defined off-axis component which persists throughout the remainder of the train of solitary waves. A longer pulse than ours would have a longer train of solitary waves and the spectral component of conical emission would saturate at a larger amplitude relative to the laser peak than shown in Fig. 11.

We chose to terminate presentation of the propagation results at this point for the reason that, after about 20% greater propagation distance, the field becomes concentrated at relatively few grid points due to continued self-focusing. Subsequently the numerical solution becomes unreliable. This problem could, of course, be solved by a numerical rescaling.

In order to define the role of the transverse coupling in the near field, an identical pulse was propagated using the annular-plane-wave approximation, Eq. (2.3). This approximation is equivalent to a set of solutions in the uni-

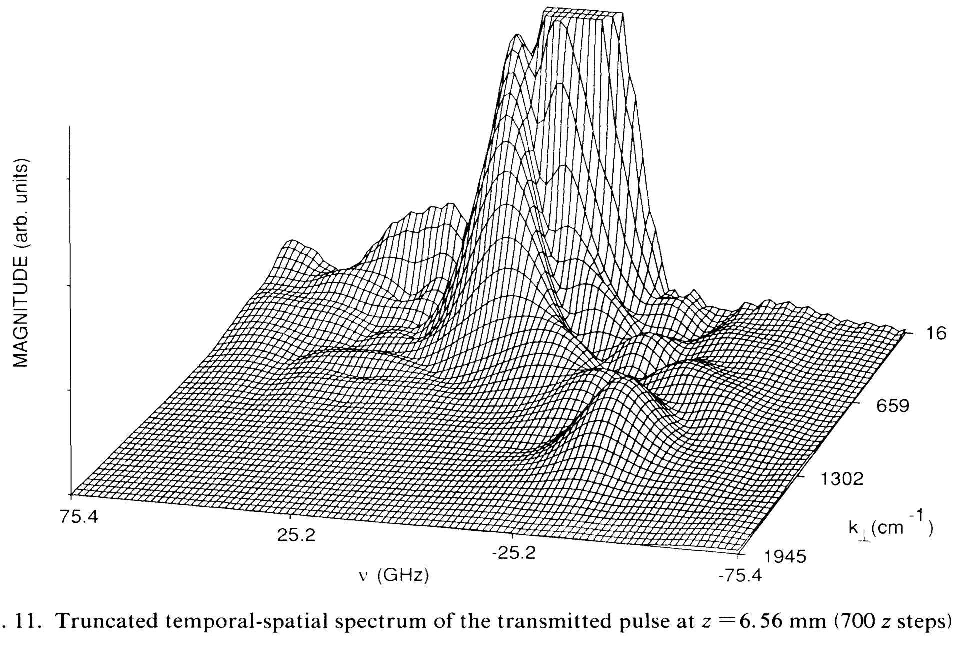

FIG. 11. Truncated temporal-spatial spectrum of the transmitted pulse at $z = 6.56$ mm (700 z steps).

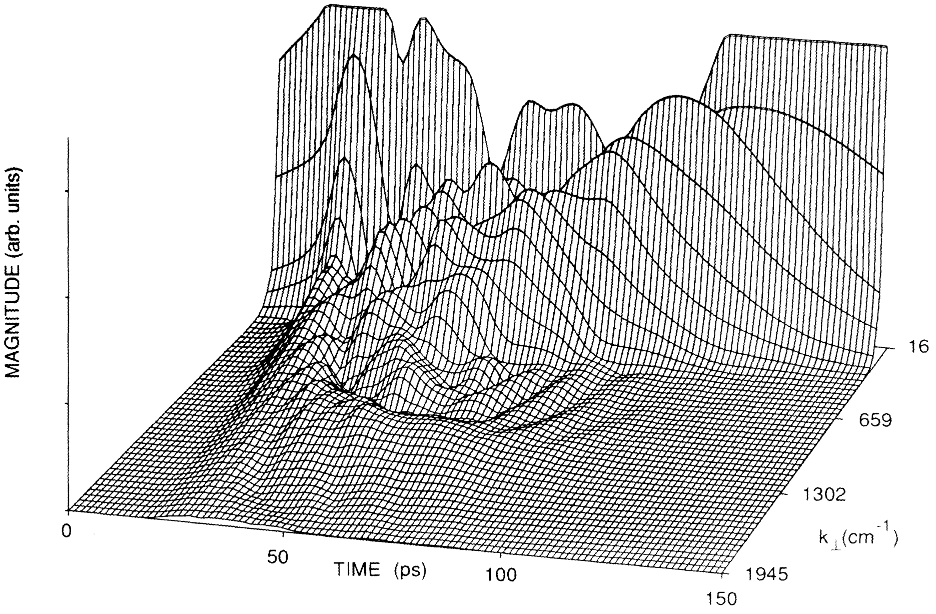

FIG. 12. Truncated magnitude of the Hankel field at $z = 6.56$ mm (700 z steps).

form plane-wave approximation for various initial vaues of peak field strength. Because each annulus is propagated independently as an uniform plane wave, only 99 radial points were used for this calculation. The dimensionless radial coordinates were chosen to be the square roots of the abscissas of the Laguerre polynomial of order 99 so that the temporal-spatial spectrum could be calculated by the same method as before. The magnitude of the field and the temporal-spatial spectrum in the annular-plane-wave approximation at $z = 6.56$ mm (700 z steps) are shown in Figs. 13 and 14. These results appear very similar to the results in the transversely coupled case, Figs. 10 and 11. This is in accordance with the fact that the Fresnel number is still relatively large, $F = 39.0$. The differences between the two sets of figures are due primarily to self-focusing, diffraction being very weak compared to the nonlinear interaction. Self-focusing increases the magnitude of the physical field strength near the axis. In addition, self-focusing enhances the rate at which all the nonlinear effects vary with radius, causing

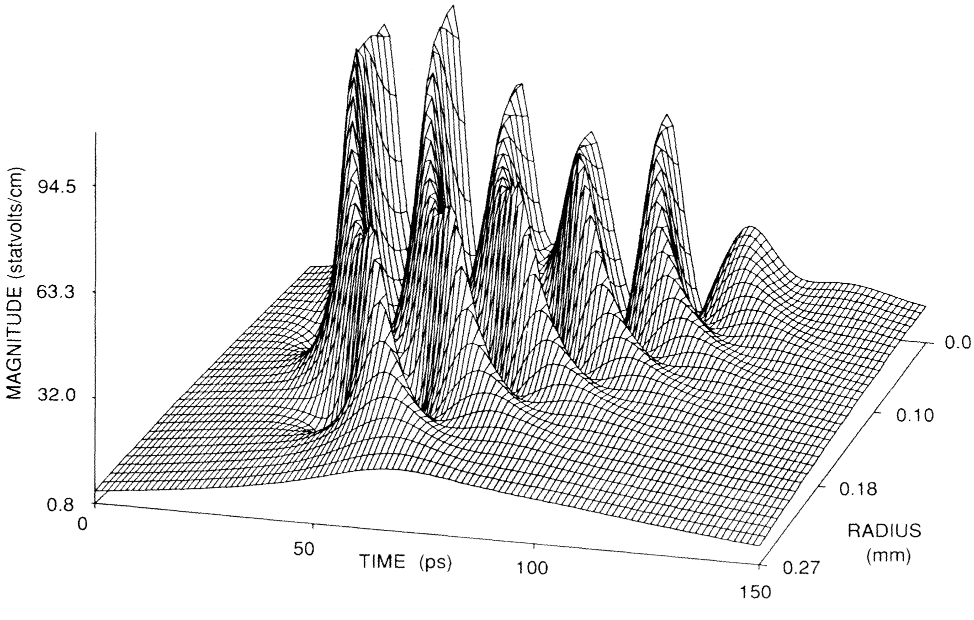

FIG. 13. Magnitude of the transmitted pulse at $z = 6.56$ mm (700 z steps) in the annular-plane-wave approximation.

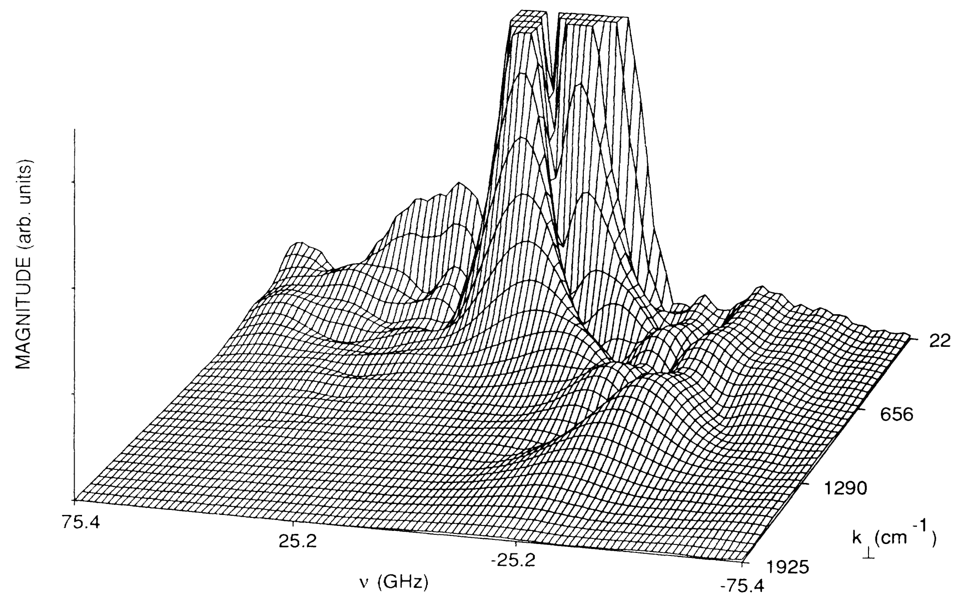

FIG. 14. Truncated temporal-spatial spectrum of the transmitted pulse at $z = 6.56$ mm (700 z steps) in the annular-plane-wave approximation.

the conical emission peak to appear at a higher transverse spatial wavenumber than in the transversely uncoupled case. The conical emission peak is closer to the laser frequency in the presence of self-focusing than in the uncoupled case because the variation of the intensity dependent velocity in the time domain is greater due to self-focusing. The influence of self-focusing and propagation distance on the transverse spatial wavenumber and temporal frequency of the conical emission peak is summarized in Fig. 15.

The development of the uniform-plane-wave solutions (shown in Fig. 16 for several values of initial peak field strength) closely parallels the development of resonant self-induced transparency.[67–69] We visualize Fig. 13 by arranging the pulses in Fig. 16 along a radial coordinate according to initial peak field strength demonstrating the correspondence between resonant self-induced transparency and the two-dimensional solitary waves shown in Figs. 10 and 13. This correspondence shows that the propagation results of Figs. 5, 6, 8, 10, and 13 can be

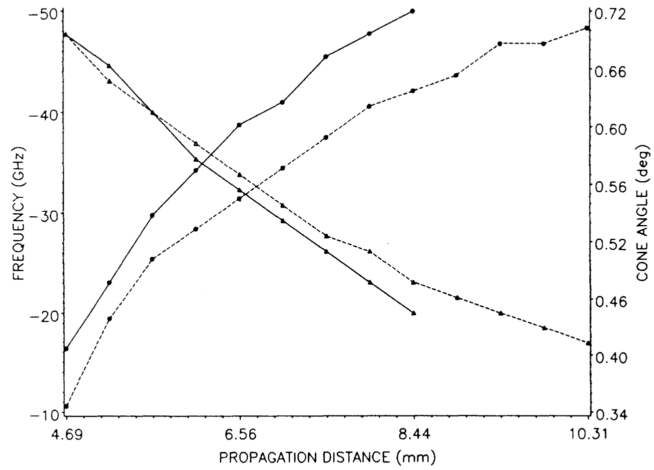

FIG. 15. Effect of the propagation distance on the half-angle (circles) and temporal frequency (triangles) on the conical emission peak. The solid lines are for transversely coupled propagation that includes the effect of self-focusing and diffraction. The annular-plane-wave approximation is represented by the dashed lines.

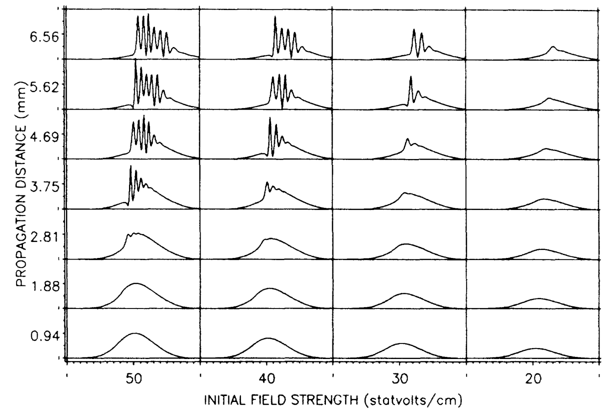

FIG. 16. Development of pulse breakup with propagation distance for different values of initial peak field strength. For each panel of the figure, the height is the magnitude of the field and the width is time. The vertical axis for each panel is 0 to 100 statvolts/cm and the horizontal axis for each panel is −200 to 200 ps.

reasonably interpreted in terms of self-induced transparency, generalized for nonresonant excitation, and for a variation of the initial field strength in the transverse dimension.

Finally, we consider the geometrical interpretation of noncollinear phase matching in the retarded-time–radius plane. Phase matching is required for constructive interference. In the case of resonant, degenerate four-wave mixing, the magnitude of the field oscillates in the radial dimension, but not in time. In the nonresonant nondegenerate case, the magnitude of the field appears like a waffle superimposed on the basic pulse shape as a result of collinear, as well as noncollinear, phase matching. Our results can be interpreted as coherent sideband generation and amplification (collinear wave mixing) with a transverse variation in the generated frequencies and index of refraction. In this model, noncollinear phase matching is a result of geometry. We conclude that a fourth parametric wave at the upper sideband frequency, which has never been observed in the conically emitted radiation (for a one-photon transition),[6,8] is not required for noncollinear phase matching.

VI. COMPARISON WITH EXPERIMENT

In this section we compare our physical model of conical emission with known experimental results. Previously performed experiments cannot be directly simulated because computer resources dictate the magnitudes of the parameters that can be considered. In addition, the laser pulses employed in the experiments performed so far were multimode and had an undesirably large temporal noise modulation. In Appendix B it is shown by scaling the equations of motion that the pulse area and $\Delta\tau$ are invariants. The total number of time points required to follow the temporal oscillations in the field is proportional to the maximum generalized Rabi frequency multiplied by the pulse length. In a loose sense, this can be related to the pulse area. The amplitude of the Rabi oscillations in the polarization relative to the total polarization varies inversely with the product $|\Delta|\tau$. As $|\Delta|\tau$ increases, more computational z steps and a higher density of radial points are required because of the longer propagation distance and the larger amount of self-focusing that occurs before pulse breakup. To deal with these computational difficulties, Mattar and Newstein[37] have developed spatial and temporal rezoning techniques for finite-difference methods which create a higher density of computational grid points in the region where the field is strongest. We have not implemented these techniques because they are not directly applicable to our Hankel algorithm.

A result of the practical restriction to a short pulse length is that very little of the pulse is near the maximum generalized Rabi frequency in our calculations. As a result, the temporal frequency at which sidebands first appear is near the detuning frequency rather than the maximum genralized Rabi frequency. Parametric studies of uniform plane-wave propagation of a Gaussian pulse with the same parameters that were used in the previous section except for a larger time FWHM show that for longer pulses sideband generation begins near the peak generalized Rabi frequency. In addition, the temporal frequency of conical emission should be larger if more self-focusing were to occur prior to beam breakup. Conical emission at a frequency significantly less than the peak generalized Rabi frequency was observed by Burdge and Lee.[11]

The paraxial approximation and the assumption of cylindrical symmetry also hinder a direct comparison between computer simulation and experiment. Cylindrical symmetry restricts the pulse to a single symmetric axial mode, whereas experimental pulses are multimode and exhibit spatial breakup into multiple filaments. The insensitivity of the cone angle to field strength[8–10] is most likely a result of spatial breakup into several focusing regions.

Doppler broadening and damping have deliberately been excluded from our calculations in order to define the smallest set of physical phenomena that can produce conical emission. While Harter, Boyd, and co-workers[6,7] based their analysis on an index of refraction calculated in the collisional steady state, Harter[71] noted that the conical emission was qualitatively the same at low atomic densities where the vapor was not collisionally broadened and where the adiabatic model should therefore be more appropriate. In our model a moderate amount of damping causes the oscillations in the polarization to decay with time.[72] Pulse breakup and conical emission proceed as described in Sec. V. Moderate damping has somewhat the same effect as the partial coherence of successive Rabi oscillations in the undamped case. Even near the steady-state limit, some transient effects will occur which accumulate and are amplified during propagation, just as we observe nonadiabatic effects near the adiabatic limit which accumulate and are amplified during propagation.[61]

Harter, Boyd, and co-workers[6,7] noted that there is a vapor-density threshold below which one observes sideband generation but not conical emission. The nonlinear interaction is directly proportional to the vapor density so that diffraction dominates the nonlinear interaction in a vapor of sufficiently low density. In this case diffraction acts to prevent conical emission by stripping away the edges of the beam. Temporal pulse breakup is allowed to progress, resulting in Rabi sidebands. Kleiber, Burnett, and Cooper[20] demonstrated that background laser fluorescence is effective in promoting sideband generation in weakly nonlinear systems. In the presence of noise, the amplitude of the oscillations in the polarization increases because the approach to the adiabatic condition is no longer an asymptotic function of $|\Delta|\tau$.[38,40] Fluorescence can provide the initial source of noise which is amplified at the sideband frequency.

In an important series of experiments, Harter and Boyd[6] studied the effect of varying the vapor density and detuning on the characteristics of the conical emission. The parameter that was studied was the minimum filament diameter $d_{\min}$, which scales as $(\Delta^3/N)^{1/2}$ in terms of the vapor density and detuning.[12] The larger the filament diameter, the weaker the nonlinear term and the greater the propagation distance required for effective self-oscillation encoding, and, therefore, the greater the beam-breakup distance. For large-diameter filaments, Harter and Boyd observed conical emission in a long vapor cell but not in a short cell. For moderate-diameter filaments, conical emission was produced along the entire length of the cell. For the smallest-diameter filament, which according to our theory should have had the shortest beam-breakup length, conical emission was generated only in the initial portion of the cell. After the cessation of conical emission, no further off-axis emission was observed and, at the end of the cell, only radiation at the laser frequency was present in the filament. Harter[71] noted that "This self-trapped filament has qualitaties similar to the solitons observed by Mollenauer in optical fibers." We propose that conical emission proceeds according to the description in Sec. V until quenched by diffraction near the self-focus. The solitary waves have different velocities and spread out, so that the sideband frequency becomes too low to be differentiated from the laser frequency. Further, the diffractive stripping of the edges of the beam leaves only the central portion of the transmitted pulse consisting of nearly straight, well-separated solitary waves so that the solitary-wave nature is readily observable.

In the general case the experimental identification of the solitary waves is difficult because of their curvature. Experimental observation of the solitary waves will require temporal resolution adequate to resolve the solitary waves (~ 10 ps under the conditions of our calculation) and near-field spatial resolution adequate to avoid averaging over the entire diameter of the beam exiting from the atomic vapor as in some previous time-resolved measurements.[6] The streak-camera measurements of Kupecek *et al.*[73] fulfill these conditions.

In our physical model, the angle of conical emission results from (1) the variation of the input field strength in the radial dimension; (2) whole-beam self-focusing prior to beam breakup, which increases the variation of the field strength in the radial dimension; (3) whole-beam self-focusing after beam breakup has begun, which compresses the solitary waves towards the axis; (4) local self-focusing and diffraction among the solitary waves; (5) radial variation in pulse velocity and self-steepening prior to beam breakup; and (6) radial variation in pulse velocity after beam breakup has begun. This categorization is somewhat arbitrary as all the processes are interrelated. However, it provides a basis for comparison with the Harter-Boyd theory[6] by separating whole-beam self-focusing, which can be modeled with an intensity-dependent index of refraction,[12,33,70] from other processes.

In the Harter-Boyd model,[6] the cone angle is given by the expression

$$\theta_c = k|2\delta n(\omega_1)|^{1/2} , \qquad (6.1)$$

where k is an adjustable constant of proportionality. The same dependence on the nonlinear index of refraction was derived by LeBerre-Rousseau, Ressayre, and Tallet[22] using a different physical model.[74] In whole-beam self-focusing the diameter of the beam at a specific propagation distance is proportional to $(\delta n)^{-1/2}$ (Ref. 70). In our model of conical emission, the cone angle varies inversely with the beam diameter so that the portion of the cone angle attributable to whole-beam self-focusing has the same dependence on δn as Eq. (6.1). On this basis, the cone opening angle is expected to decrease as the detuning increases and to increase as the vapor density increases. Both of these effects are well known.[6–10,13,14,16,19]

Once the field amplitude develops temporal-spatial oscillations, the intensity-dependent index of refraction induces temporal-spatial oscillations in the phase with a smaller depth of modulation. This causes local self-focusing and diffraction among the solitary waves because the transverse energy flow due to the transverse derivative of the phase redistributes energy in a manner analogous to coherent resonant self-focusing.[36,37]

Transverse energy flow is not the only contributor to the cone angle. There is a significant cone angle even without transverse coupling as demonstrated by Fig. 15. The latter contribution to the cone angle depends on both the initial variation of the field strength at the entrance to the medium and the variation of the intensity-dependent pulse velocity in the radial dimension.

The observed shift of the transmitted laser frequency to the blue[9] and the spatial broadening[8–10] of the central spot have been previously attributed to self-phase modulation.[8,10] This is borne out by Figs. 7, 9, and 11, which show that the temporal frequency is pulled to the blue and the spatial frequency spectrum is broadened under propagation.

The unusually broad spectral width of the conical emission noted by most experimentalists[8–10,14] is a result of the variation of the generalized Rabi frequency in time and radius. Contributions from a number of focusing regions with different field strengths would result in still further broadening. The observed asymmetry of the sideband has been attributed to incoherent reabsorption by the vapor,[8,13] which was not included in our model. Finally, since the spatial and temporal frequency of conical emission vary with propagation distance, we would expect contributions from a range of frequencies even given only a single focusing region. The latter effect has been observed as an angular distribution of frequencies within the cone.[13,15]

The sideband asymmetry produced by self-oscillation encoding changes sign with the detuning. We would therefore expect to see conical emission at the upper sideband frequency for a self-defocusing pulse. However, for a pulse undergoing self-defocusing as well as diffraction the decay in field strength delays, and may even prevent, pulse breakup. If pulse breakup occurs after significant lateral spreading, the spatial frequency may be too low to permit conical emission to be distinguished from beam broadening. However, for a two-photon transition in a three-level system, where self-defocusing due to a red detuning of one transition is offset by self-focusing due to a blue detuning of a second transition, we would expect to see conical emission at both upper and lower sidebands, an effect which has been observed experimentally.[19]

ACKNOWLEDGMENTS

The authors thank C. A. Glosson for coding the Hankel transformation in Cray and Convex assembly languages and N. R. Davis, S. T. Garner, and C. S. Milsted, Jr. for writing portions of the pre- and post-processing software. This research was supported by the U.S. Office of Naval Research, the National Science Foundation (Grant No. PHY-8519293), Cray Research, Inc., Convex Computer Corporation, and the Texas Advanced Technology and Research Program (Grant No. UD-011). Computational resources for this research were provided by the University of Texas System Center for High Performance Computing and the University of Texas at Dallas.

APPENDIX A

In this appendix we show in detail how the transient nonlinear interaction and diffraction determine the phase surface and reshape the field. Both self-focusing and self-steepening can be analyzed semiquantitatively by examining the modulated phase front produced by optical nonlinearity and diffraction, in the limit in which the incident pulse is sufficiently adiabatic for Eq. (4.1) to be valid.

The complex field can be expressed as a positive magnitude multiplied by a phasor

$$E(r,z,t')=\mathcal{E}(r,z,t')e^{i\phi(r,z,t')} , \tag{A1}$$

where $\mathcal{E}(r,z,t')=|E(r,z,t')|$ and t' is the retarded time. The propagating field can then be written as

$$\mathsf{E}(r,z,t)=\mathcal{E}(r,z,t')e^{i\zeta(r,z,t)} , \tag{A2}$$

where

$$\zeta(r,z,t)=k_l z-\omega_l t+\phi(r,z,t') . \tag{A3}$$

In the calculation of the phase, k_l and ω_l are fixed; only ϕ varies. It is useful to consider the contributions of optical nonlinearity and diffraction separately, replacing the variation of $\phi(r,z,t')$ as calculated numerically by a variation due to the approximate nonlinear response and to the process of diffraction. In this model, the phase of the propagating field is

$$\zeta(r,z,t)=\frac{\omega_l}{c}n(r,z,t)z-\omega_l t+\frac{r^2 z}{2k_l a_0^4\sec^2[\psi(z)]}-\psi(z) , \tag{A4}$$

where

$$\psi(z)=\tan^{-1}\left[\frac{z}{k_l a_0^2}\right] . \tag{A5}$$

The index of refraction can be written as

$$n=(1+4\pi\chi)^{1/2}\approx 1+2\pi\chi \tag{A6}$$

provided that $4\pi\chi \ll 1$. The latter inequality can be satisfied only when $n_0\approx 1$. For $n_0=1$ the phase of the complex field as a function of retarded time,

$$\phi(r,z,t')\approx 2\pi\frac{\omega_l}{c}\chi(r,z,t')z+\frac{r^2 z}{2k_l a_0^4\sec^2[\psi(z)]}-\psi(z) , \tag{A7}$$

can be deduced from Eqs. (A3), (A4), and (A6).

The susceptibility is to be calculated from the expression for the second-order approximation to the polarization, Eq. (4.1). For almost any pulse of interest, the inverse square root in Eq. (4.2) can be approximated by the first two terms of the binomial expansion. In this approximation and for an attenuating medium, the second-order susceptibility $\chi_{(2)}=P_{(2)}/iE$ becomes

$$\begin{aligned}\chi_{(2)}\approx \frac{N\mu^2|\Delta|}{\hbar}&\left[-\frac{\Omega'^2}{\Delta}-\frac{\mu^2\mathcal{E}^2}{2\hbar^2}\frac{d\phi}{dt'}-\frac{d\phi}{dt'}+\frac{i}{\mathcal{E}}\frac{d\mathcal{E}}{dt'}\right]\\ &\times\left\{\frac{1}{\Omega'^3}-\frac{\mu^2\Delta^2}{2\hbar^2\Omega'^9}\left[\left[\frac{d\mathcal{E}}{dt'}\right]^2+\mathcal{E}^2\left[\frac{d\phi}{dt'}\right]^2\right]\right.\\ &\left.\quad-\frac{\mu^2\mathcal{E}^2}{\Delta\hbar^2\Omega'^5}\frac{d\phi}{dt'}-\frac{2\Delta^2\hbar^2\mu^4\mathcal{E}^4+\mu^6\mathcal{E}^6}{2\Delta^2\hbar^6\Omega'^9}\left[\frac{d\phi}{dt'}\right]^2\right\}\end{aligned} \tag{A8}$$

in terms of the magnitude and phase defined by Eq. (A1). The susceptibility $\chi_{(2)}$, which is calculated using the adiabatic approximation with a correction term, is not related to $\chi^{(2)}$ in the expansion of the susceptibility in powers of the electric field. Our approximate $\chi_{(2)}$ contains all powers of the electric field.

Most of the interesting properties of the phase appear at the entrance to the medium, where $d\phi/dt'=0$ and Eq. (A8) has a simpler form. Further, we assume $\mu^2\mathcal{E}^2/\Delta^2\hbar^2 \ll 1$ which is true for the entire time-radius plane, except possibly near the peak. This allows the first two terms of the binomial expansion to be used in expanding the generalized Rabi frequency. Neglecting terms higher than first order in $d\mathcal{E}/dt'$, we obtain the approximate susceptibility

$$\chi_{(2)}\approx\frac{N\mu^2}{\hbar}\left[-\frac{1}{\Delta}+\frac{\mu^2\mathcal{E}^2}{2\Delta^3\hbar^2}+\frac{i}{\Delta^2}\frac{\dot{\mathcal{E}}}{\mathcal{E}}-\frac{3i}{2}\frac{\mu^2\mathcal{E}\dot{\mathcal{E}}}{\Delta^4\hbar^2}\right] . \tag{A9}$$

The first term in Eq. (A9) is constant and will not be considered further. The second term is an intensity-dependent index of refraction and produces a nonlinearly-generated image of the intensity profile of the pulse in the phase surface. The image is concave downward for positive detuning and concave upward for negative detuning. For a Gaussian pulse, $\dot{\mathcal{E}}/\mathcal{E}$ is $-t'/\tau^2$. Therefore the third term in Eq. (A9) is responsible for gain when t' is less than zero and absorption when t' is greater than zero. For the approximate susceptibility given by Eq. (A9), Eq. (A7) predicts a phase surface (as a function of r and t', for a given z) that is simply the sum of a positive (or negative) image of the intensity and the parabolic phase front expected for propagation in free space. Higher-order terms in the polarization make additional contributions to the phase surface.

The transverse dependence of the intensity-dependent index of refraction δn is responsible for whole-beam self-focusing (or self-defocusing).[12,33,70] From Eq. (A9), we obtain the intensity-dependent index of refraction

$$\delta n \approx \frac{\pi N \mu^4 \mathcal{E}^2}{\Delta^3 \hbar^3} \tag{A10}$$

to first order. In early work, such a Kerr-type intensity-dependent index of refraction was used to predict pulse reshaping by an intensity-dependent pulse velocity.[32] This analysis predicts that the trailing edge of the pulse will steepen when the detuning is positive and the leading edge will steepen when the detuning is negative. Later calculations substantially altered this view when the dispersion caused by self-phase modulation was introduced into the analysis. Grischkowsky[29] made a fully coherent calculation of the group velocity using the adiabatic approximation. The group velocity is calculated using the relationships

$$\frac{1}{v_g} = \frac{dk}{d\omega} = \frac{1}{c}\left[1 + 2\pi\chi + 2\pi\omega\frac{d\chi}{d\omega}\right] . \tag{A11}$$

We use the second-order approximation for the susceptibility to obtain

$$\frac{c}{v_g} \approx 1 + \frac{N\mu^2|\Delta|}{\hbar\Omega'^3}\left\{1 - \frac{\mu^2\dot{\mathcal{E}}^2}{2\hbar^2\Omega'^6}\left[5\Delta^2 - \frac{2\mu^2\mathcal{E}^2}{\hbar^2}\right] - \frac{\mu^2\mathcal{E}^2\dot{\phi}}{\hbar^2\Delta^3\Omega'^2}\left[4\Delta^2 + \frac{\mu^2\mathcal{E}^2}{\hbar^2}\right] - \frac{\mu^2\mathcal{E}^2\dot{\phi}^2}{2\hbar^2\Omega'^6}\left[5\Delta^2 + \frac{12\mu^2\mathcal{E}^2}{\hbar^2} + \frac{\mu^4\mathcal{E}^4}{\hbar^4}\left[9\Delta^2 + \frac{2\mu^2\mathcal{E}^2}{\hbar^2}\right]\right]\right\} . \tag{A12}$$

For a nearly adiabatic pulse, only the unit term in the braces is significant. In this approximation the more intense parts of the pulse travel faster, so that the pulse undergoes self-steepening. The higher-order terms amplify self-steepening until an optical shock[31,32] develops. The higher-order terms then begin to act as limiters. Since $d\phi/dt'$ is an odd function of Δ, self-steepening occurs in the same manner on both sides of the resonance line to at least second order.

The intensity-dependent pulse velocity does not provide an additional self-steepening mechanism in addition to the gain and absorption described by Eqs. (A8) and (A9). Rather, Eqs. (A8) and (A9) show how self-steepening and pulse delay are manifested in the course of numerical propagation. While an intensity-dependent group velocity can be calculated based on the adiabatic approximation, using the adiabatic polarization as the source term in the wave equation results in a pulse that travels at c/n_0. The higher-order terms in the polarization are necessary to effect self-steepening and pulse delay.

APPENDIX B

Our graphical results can be applied to related problems and one's physical understanding can be enhanced by scaling Schrödinger's equation and the paraxial wave equation. Define a dimensionless time $\tau = t'/\tau_p$, a dimensionless field $\varepsilon = \mu E \tau_p / 2\hbar$, a dimensionless radius $\rho = r/r_p$, and a dimensionless length $\eta = 2\pi\omega_l N \mu^2 \tau_p z / c\hbar n_0$, where τ_p is a characteristic pulse time and $r_p = a_0(2\ln 2)^{1/2}$ is the radius half-maximum. Equations (2.5, 2.6, and 2.1) become

$$\frac{\partial \tilde{c}_0}{\partial \tau} = i\varepsilon^* \tilde{c}_1 , \tag{B1}$$

$$\frac{\partial \tilde{c}_1}{\partial \tau} = i\Delta\tau_p \tilde{c}_1 + i\varepsilon\tilde{c}_0 , \tag{B2}$$

$$\left[\frac{-i\hbar c^2}{4\pi N \tau_p \mu^2 \omega_l^2 r_p^2}\nabla^2_{T,\rho} + \frac{\partial}{\partial \eta}\right]\varepsilon = i\tilde{c}_0^* \tilde{c}_1 . \tag{B3}$$

Equations (B1), (B2), and (B3) show that when the problem is stated in terms of the dimensionless independent variables τ, η, and ρ and the dimensionless dependent variable ε, the answer is completely determined by the dimensionless constants (i) $\mu E_0 \tau_p / 2\hbar$, (ii) $\Delta\tau_p$, and (iii) $\hbar c^2 / 4\pi\mu^2\omega_l^2 \tau_p N r_p^2$ for the same form of pulse envelope. Condition (i) requires a constant pulse area. Condition (ii) requires that the angular velocity of the Bloch vector about the torque vector in a coordinate system rotating with the torque vector also remain constant. Conditions (i) and (ii) can be combined to obtain the dimensionless constants (iv) $\mu E_0 / \Delta\hbar$ and (v) as follows:

$$\frac{\Omega'}{\Delta} = \left[1 + \left[\frac{\mu E_0}{\Delta\hbar}\right]^2\right]^{1/2} .$$

Conditions (iv) and (v) require that the Rabi frequency and the ratio of the generalized Rabi frequency to the detuning frequency remain constant. Thus all frequencies maintain a constant relationship to one another. Condition (iii) can be combined with the dimensionless length η to show that the Fresnel number (vi)

$$F = \frac{\pi r_p^2}{(\lambda/n_0)L} ,$$

where (λ/n_0) is the wavelength in the medium and $r_p = a_0(2\ln 2)^{1/2}$ is the radius half-maximum, does not change under rescaling.

[1] B. R. Mollow, Phys. Rev. **188**, 1969 (1969); Phys. Rev. A **2**, 76 (1970); H. J. Kimble and L. Mandel, *ibid.* **13**, 2123 (1976); F. Schuda, C. R. Stroud, Jr., and M. Hercher, J. Phys. B **7**, L198 (1974); F. Y. Wu, R. E. Grove, and S. Ezekiel, Phys. Rev. Lett. **35**, 1426 (1975); H. Walther, in *Laser Spectroscopy,* edited by S. Haroche *et al.* (Springer-Verlag, Berlin, 1975), p. 358; H. M. Gibbs and T. N. C. Venkatesan, Opt. Commun. **17**, 87 (1976); R. E. Grove, F. Y. Wu, and S. Ezekiel, Phys. Rev. A **15**, 227 (1977); W. Hartig, W. Rasmussen, R. Schieder, and H. Walther, Z. Phys. A **278**, 205 (1977).

[2] H. M. Gibbs, S. L. McCall, and T. N. C. Venkatesan, Phys. Rev. Lett. **36**, 1135 (1976); F. Y. Wu, S. Ezekiel, M. Ducloy, and B. R. Mollow, *ibid.* **38**, 1077 (1977).

[3] A. C. Tam, Phys. Rev. A **19**, 1971 (1979).

[4] S. L. McCall, Phys. Rev. A **9**, 1515 (1974).

[5] S. G. Rautian and I. I. Sobel'man, Zh. Eksp. Teor. Fiz. **41**, 456 (1961) [Sov. Phys.—JETP **14**, 328 (1962)]; S. Haroche and F. Hartmann, Phys. Rev. A **6**, 1280 (1972); B. R. Mollow, *ibid.* **5**, 2217 (1972); M. Sargent III and P. E. Toschek, Appl. Phys. **11**, 107 (1976); C. Cohen-Tannoudji and S. Reynaud, J. Phys. B **10**, 345 (1977).

[6] D. J. Harter and R. W. Boyd, Phys. Rev. A **29**, 739 (1984).

[7] D. J. Harter, P. Narum, M. G. Raymer, and R. W. Boyd, Phys. Rev. Lett. **46**, 1192 (1981).

[8] C. H. Skinner and P. D. Kleiber, Phys. Rev. A **21**, 151 (1980).

[9] Y. H. Meyer, Opt. Commun. **34**, 439 (1980).

[10] G. Brechignac, Ph. Cahuzac, and A. Debarre, Opt. Commun. **35**, 87 (1980).

[11] G. L. Burdge and C. H. Lee, Appl. Phys. B **28**, 197 (1982).

[12] D. Grischkowsky, Phys. Rev. Lett. **24**, 866 (1970).

[13] E. A. Chauchard and Y. H. Meyer, Opt. Commun. **52**, 141 (1984).

[14] I. Golub, R. Shuker, and G. Erez, Opt. Commun. **57**, 143 (1986).

[15] A. I. Plekhanov, S. G. Rautian, V. P. Safonov, and B. M. Chernobrod, Zh. Eksp. Teor. Fiz. **88**, 426 (1985) [Sov. Phys.—JETP **61**, 249 (1985)]; Pis'ma Zh. Eksp. Teor. Fiz. **36**, 232 (1982) [JETP Lett. **36**, 284 (1983)].

[16] I. Golub, G. Erez, and R. Shuker, J. Phys. B **19**, L115 (1986).

[17] Y. Shevy and M. Rosenbluh, J. Opt. Soc. Am. B **5**, 116 (1988).

[18] Y. Shevy, S. Hochman, and M. Rosenbluh, Opt. Lett. **13**, 215 (1988).

[19] J. Krasinski, D. J. Gauthier, M. S. Malcuit, and R. W. Boyd, Opt. Commun. **54**, 241 (1985); M. S. Malcuit, D. J. Gauthier, and R. W. Boyd, Phys. Rev. Lett. **55**, 1086 (1985); R. W. Boyd, M. S. Malcuit, D. J. Gauthier, and K. Rzążewski, Phys. Rev. A **35**, 1648 (1987); V. Vaĭchaĭtis, M. Ignatavichyus, V. A. Kudryashov, Yu. N. Pimenov, and R. Yakite, Kvant. Elektron. **14**, 762 (1987) [Sov. J. Quantum Electron. **17**, 478 (1987)].

[20] P. D. Kleiber, K. Burnett, and J. Cooper, Phys. Rev. A **25**, 1188 (1982).

[21] S. D. Durbin, S. M. Arakelian, and Y. R. Shen, Opt. Lett. **6**, 411 (1981).

[22] M. LeBerre-Rousseau, E. Ressayre, and A. Tallet, Opt. Commun. **36**, 31 (1981).

[23] A. A. Makarov, C. D. Cantrell, and W. H. Louisell, Opt. Commun. **31**, 31 (1979); C. D. Cantrell, W. H. Louisell, and A. A. Makarov, in *Photoselective Chemistry,* edited by J. Jortner, R. Levine, and S. A. Rice (Wiley, New York, 1980), pp. 583–624.

[24] For a general review of laser-induced chemical reactions and isotope separation, see (a) C. D. Cantrell, S. M. Freund, and J. L. Lyman, in *The Laser Handbook,* edited by M. L. Stitch (North-Holland, Amsterdam, 1979), Vol. III, pp. 485–576; (b) V. S. Letokhov and C. B. Moore, Kvant. Elektron. **3**, 248 (1976) [Sov. J. Quantum Electron. **6**, 129 (1976)]; *ibid.* **3**, 485 (1976) [*ibid.* **6**, 259 (1976)].

[25] J. H. Eberly, M. J. Konopnicki, and B. W. Shore, Opt. Commun. **35**, 76 (1980).

[26] C. D. Cantrell, F. Rebentrost, and W. H. Louisell, Opt. Commun. **36**, 303 (1981).

[27] M. E. Crenshaw and C. D. Cantrell, Opt. Lett. **13**, 386 (1988).

[28] M. E. Crenshaw, C. D. Cantrell, C. A. Glosson, and D. D. Chu, in *Science and Engineering on Cray Supercomputers,* Proceedings of the Third International Symposium, Minneapolis, 1987 edited by J. E. Aldag (Cray Research, Minneapolis, 1987), pp. 477–490; M. E. Crenshaw and C. D. Cantrell, in *Conference on Lasers and Electro-Optics Technical Digest Series 1988, Vol. 7* (Optical Society of America, Washington, D.C., 1988), pp. 146 and 147.

[29] D. Grischkowsky, in *Laser Applications to Optics and Spectroscopy,* edited by S. F. Jocobs, M. Sargent III, J. F. Scott, and M. O. Scully (Addison-Wesley, Reading, MA, 1975), pp. 437–452.

[30] Y. R. Shen, Prog. Quantum Electron. **4**, 1 (1975).

[31] D. Grischkowsky, E. Courtens, and J. A. Armstrong, Phys. Rev. Lett. **31**, 422 (1973).

[32] F. DeMartini, C. H. Townes, T. K. Gustafson, and P. L. Kelley, Phys. Rev. **164**, 312 (1967).

[33] T. K. Gustafson, J. P. Taran, H. A. Haus, J. R. Lifsitz, and P. L. Kelley, Phys. Rev. **177**, 306 (1969).

[34] F. A. Hopf and M. O. Scully, Phys. Rev. **179**, 399 (1969).

[35] A. Icsevgi and W. E. Lamb, Jr., Phys. Rev. **185**, 517 (1969).

[36] N. Wright and M. C. Newstein, Opt. Commun. **9**, 8 (1973).

[37] F. P. Mattar and M. C. Newstein, in *Cooperative Effects in Matter and Radiation,* edited by C. M. Bowden, D. W. Howgate, and H. R. Robl (Plenum, New York, 1977), pp. 139–192; Comput. Phys. Commun. **20**, 139 (1980); Opt. Commun. **18**, 70 (1976); IEEE J. Quantum Electron. **QE-13**, 507 (1977); F. P. Mattar *et al.*, in *Coherence and Quantum Optics,* edited by L. Mandel and E. Wolf (Plenum, New York, 1978), pp. 143–164.

[38] G. L. Peterson and C. D. Cantrell, Phys. Rev. A **31**, 807 (1985).

[39] M. LeBerre, E. Ressayre, A. Tallet, and F. P. Mattar, J. Opt. Soc. Am. B **2**, 956 (1985).

[40] M. E. Crenshaw and C. D. Cantrell, Phys. Rev. A **37**, 3338 (1988).

[41] E. Courtens and A. Szöke, Phys. Rev. A **15**, 1588 (1977); **17**, 2119 (1978).

[42] J. H. Eberly, C. V. Kunasz, and K. Wódkiewicz, J. Phys. B **13**, 217 (1980).

[43] B. Renaud, R. M. Whitley, and C. R. Stroud, Jr., J. Phys. B **10**, 19 (1977).

[44] G. Nienhuis, Physica B+C **96C**, 391 (1979).

[45] M. LeBerre, E. Ressayre, and A. Tallet, Phys. Rev. A **25**, 1604 (1982).

[46] M. Sargent III, M. O. Scully, and W. E. Lamb, Jr., *Laser Physics* (Addison-Wesley, Reading, MA, 1974).

[47] B. J. Coffey, M. Lax, and C. J. Elliot, IEEE J. Quantum Electron. **QE-19**, 297 (1983).

[48] D. Gottlieb, M. Y. Hussaini, and S. A. Orszag, in *Spectral Methods for Partial Differential Equations,* edited by R. G. Voigt, D. Gottlieb, and M. Y. Hussaini (Society for Industrial and Applied Mathematics, Philadelphia, 1984), pp. 1–54.

[49] *Higher Transcendental Functions,* edited by A. Erdélyi (Krieger, Malabar, FL, 1985), Vol. II, p. 189.

[50] The abscissas and weights were calculated using a program listed by A. H. Stroud and D. Secrest, *Gaussian Quadrature Formulas* (Prentice-Hall, Englewood Cliffs, NJ, 1966). Note that the normalization of the Laguerre polynomials differs from that of Ref. 49.

[51] M. D. Crisp, Phys. Rev. A **8**, 2128 (1973).

[52] S. Osher, in *Spectral Methods for Partial Differential Equations*, edited by R. G. Voight, D. Gottlieb, and M. Y. Hussaini (Society for Industrial and Applied Mathematics, Philadelphia, 1984), pp. 209–216.

[53] D. D. Chu and C. D. Cantrell (unpublished).

[54] L. Lapidus and J. H. Seinfeld, *Numerical Solution of Ordinary Differential Equations* (Academic, New York, 1971).

[55] N. Danesh and C. D. Cantrell (private communication).

[56] P. D. Drummond, Comput. Phys. Commun. **29**, 211 (1983).

[57] L. Allen and J. H. Eberly, *Optical Resonance and Two-Level Atoms* (Dover, New York, 1987), pp. 72–77.

[58] A. Messiah, *Quantum Mechanics* (North-Holland, Amsterdam, 1962), Vol. II, pp. 749–751.

[59] D. Grischkowsky, Phys. Rev. A **7**, 2096 (1973).

[60] H. J. Kimble and L. Mandel, Phys. Rev. A **15**, 689 (1977).

[61] P. L. Knight, W. A. Molander, and C. R. Stroud, Jr., Phys. Rev. A **17**, 1547 (1978); P. L. Knight and P. W. Milonni, Phys. Rep. **66**, 21 (1980).

[62] D. J. Kaup, Phys. Rev. A **16**, 704 (1977).

[63] V. E. Zakharov and A. B. Shabat, Zh. Eksp. Teor. Fiz. **61**, 118 (1971) [Sov. Phys.—JETP **34**, 62 (1972)].

[64] R. G. Brewer and R. L. Shoemaker, Phys. Rev. A **6**, 2001 (1972).

[65] W. E. Lamb, Jr., Phys. Rev. **134**, A1429 (1964).

[66] V. G. Makhankov, Phys. Rep. **35**, 1 (1978).

[67] S. L. McCall and E. L. Hahn, Phys. Rev. Lett. **18**, 908 (1967); Phys. Rev. **183**, 457 (1969).

[68] G. L. Lamb, Jr., Rev. Mod. Phys. **43**, 99 (1971).

[69] R. E. Slusher and H. M. Gibbs, Phys. Rev. A **5**, 1634 (1972); **6**, 1255 (1972).

[70] A. Javan and P. L. Kelley, IEEE J. Quantum Electron. **QE-2**, 470 (1966).

[71] D. J. Harter, Ph.D. thesis, University of Rochester, Rochester, NY, 1982.

[72] M. E. Crenshaw and C. D. Cantrell (unpublished); N. R. Davis and C. D. Cantrell (private communication).

[73] Ph. Kupecek, M. Comte, J.-P. Marinier, J.-P. Babuel-Peyrissac, and C. Bardin, Opt. Commun. **65**, 306 (1988).

[74] C. H. Skinner, Opt. Commun. **41**, 255 (1982).